— -714

学位論文

Coagulation factor XI induces Ca^{2+} response and accelerates cell migration in vascular smooth muscle cells via proteinase-activated receptor 1

香川大学大学院医学系研究科
分子情報制御医学専攻

劉文華

Title: Coagulation factor XI induces Ca^{2+} response and accelerates cell migration in vascular smooth muscle cells via proteinase-activated receptor 1

Running Head: Vascular smooth muscle effect of FXIa

Authors and affiliation: Wenhua Liu, Takeshi Hashimoto, Tetsuo Yamashita, Katsuya Hirano

Department of Cardiovascular Physiology, Faculty of Medicine, Kagawa University, Kagawa, Japan

Corresponding author: Katsuya Hirano, MD, PhD, Professor.
Department of Cardiovascular Physiology, Faculty of Medicine, Kagawa University, 1750-1 Ikenobe, Miki-cho, Kita-gun, Kagawa, 761-0793, Japan. Tel: +81-87-891-2100, Fax: +81-87-891-2101, E-mail: khirano@med.kagawa-u.ac.jp

Author Contributions

All authors contributed to design of the work, acquisition, analysis and interpretation of the data, and drafting the manuscript. All authors approved the final version of the manuscript and agreed to be accountable for all aspects of the work in ensuring that questions related to accuracy and integrity of any part of the work are appropriately investigated and resolved. All authors thus qualify for authorship.

Abstract

Activated coagulation factor XI (FXIa) is a serine proteinase that plays a key role in the intrinsic coagulation pathway. The analysis of FXI-knockout mice has indicated the contribution of FXI to the pathogenesis of atherosclerosis. However, the underlying mechanism remains unknown. We hypothesized that FXIa exerts vascular smooth muscle effects via proteinase-activated receptor 1 (PAR_1). Fura-2 fluorometry revealed that FXIa elicited intracellular Ca^{2+} signal in rat embryo aorta smooth muscle A7r5 cells. The influx of extracellular Ca^{2+} played a greater role in generating Ca^{2+} signal than the Ca^{2+} release from intracellular stores. The FXIa-induced Ca^{2+} signal was abolished by the pretreatment with atopaxar, an antagonist of PAR_1, or 4-amidinophenylmethanesulfonyl fluoride (p-APMSF), an inhibitor of proteinase, while it was also lost in embryonic fibroblasts derived from $PAR_1^{-/-}$ mice. FXIa cleaved the recombinant protein containing the extracellular region of PAR_1 at the same site (R45/S46) as that of thrombin, a canonical PAR_1 agonist. The FXIa-induced Ca^{2+} influx was inhibited by diltiazem, an L-type Ca^{2+} channel blocker, and by siRNA targeted to $Ca_V1.2$. The FXIa-induced Ca^{2+} influx was also inhibited by GF109203X and rottlerin, inhibitors of protein kinase C. In a wound healing assay, FXIa increased the rate of cell migration by 2.46-fold of control, which was partly inhibited by atopaxar or diltiazem. In conclusion, FXIa mainly elicits Ca^{2+} signal via the PAR_1/$Ca_V1.2$-mediated Ca^{2+} influx and accelerates the migration in vascular smooth muscle cells. The present study provides the first evidence that FXIa exerts a direct cellular effect on vascular smooth muscle.

Keywords: Coagulation factor XI, Proteinase-activated receptor, vascular smooth muscle

Abbreviations: ANOVA, analysis of variance; CaMKII, Ca^{2+}/calmodulin-dependent protein kinase II: $[Ca^{2+}]_i$, cytosolic Ca^{2+} concentrations; DMEM, Dulbecco's modified Eagle medium; DTT, dithiothreitol; FXI, coagulation factor XI; FXIa, activated FXI; GST, glutathione S-transferase; HBS, hepes-buffered saline solution; HK, high molecular weight kininogen; MEF, mouse embryonic fibroblasts; p-APMSF, 4-amidinophenylmethanesulfonyl fluoride; PAR, proteinase-activated receptor; PAR_1-AP, PAR_1-activating peptides; PAR_2-AP, PAR_2-activating peptides; PAR_1E, extracellular region of PAR_1; PI3-kinase, phosphatidyl-inositol 3-kinase; PKA, protein kinase A; PKC, protein kinase C; PMSF, phenylmethylsulfonyl fluoride; SOCE, store-operated Ca^{2+} entry; RT, reverse transcription; TRP, transient receptor potential.

Introduction

Coagulation factor XI (FXI) plays a key role in the intrinsic coagulation pathway. FXI is activated upon cleavage at R^{369}-I^{370} by FXIIa or thrombin or via a mechanism of autocatalytic activation (7, 25). Activated FXI (FXIa) exhibits serine proteinase activity and cleaves a downstream factor IX. FXI exists as a 160-kDa disulfide-linked homodimer of 607-amino acid subunit, each of which contains four 90- or 91-amino acid repeats called apple domains (A1 to A4 from the N-terminus) and a C-terminal trypsin-like catalytic domain (4). FXI dimer circulates in blood as a complex with a high molecular weight kininogen (HK) (4). The dimer formation is unique to FXI in comparison to other coagulation factors.

FXI-knockout mice exhibits no prolongation of bleeding time after tail transection (9). In contrast, $FeCl_3$-induced thrombus formation is markedly impaired in FXI knockout mice (27, 28). Thus, FXI appears to play a more important role in pathological thrombus formation than in physiological hemostasis (43). FXI is therefore anticipated to be a potential target for developing a new anticoagulant that inhibits thrombus formation, with less bleeding (8, 42).

FXI gene knockout was further shown to attenuate the development of high fat diet-induced atherosclerotic lesions in apolipoprotein E knockout mice (33). Analysis of FXI-knockout mice also revealed the contribution of FXI to the development of inflammation in a sepsis model and the migration of inflammatory cells (15, 37). However, it remains unclear whether these atherogenic and proinflammatory effects of FXI are attributed to its function as a coagulation factor or any direct cellular effect.

Thrombin, FVIIa, and FXa are known to activate proteinase-activated receptors (PARs) and exert direct cellular effects, thereby contributing to atherosclerosis (12, 29). PARs belong to a G protein-coupled receptor family, and 4 subtypes have been identified (2). These receptors exhibit unique mechanisms of activation. The cleavage of the extracellular N-terminal region at the defined sites by agonist proteinases unveils a new N-terminus, which acts as a tethered ligand and activates the receptor (2, 45). The synthetic peptides corresponding to the ligand region are capable of activating the receptors in a subtype-specific manner, independently of proteolytic cleavage. These peptides are therefore referred to as PAR-activating peptides (2, 45). Among 4 subtypes, PAR_1, PAR_3 and PAR_4 serve as a receptor for thrombin (12). PAR_3 has no signaling activity *per se*; PAR_4 lacks a hirudin-like domain that endorses a high affinity to thrombin (2). Thus, PAR_1 serves as a high-affinity, signaling receptor for thrombin. In blood vessel, PAR_1 mediates the thrombin-induced vascular effects, such as endothelial barrier dysfunction, contraction of smooth muscle, and acceleration of smooth muscle cell migration (12, 32, 38). However, whether FXIa can activate PARs to exert a vascular effect is unknown.

The present study, using cultured vascular smooth muscle cells, addresses the hypothesis that FXIa exerts cellular effects via PARs in vascular smooth muscle cells. Fura-2 fluorometry demonstrated that FXIa mainly elicited intracellular Ca^{2+} signal due to the PAR_1-mediated activation of the voltage-operated Ca^{2+} channel. Functionally, a wound healing assay demonstrated that FXIa accelerated the migration of vascular smooth muscle cells in a manner that was partly dependent on PAR_1 and Ca^{2+} signaling. The present study provides the first experimental evidence to support that FXIa exerts direct effects on vascular smooth muscle.

Materials and Methods

Ethical approval

The experimental protocol was approved by the Kagawa University Institutional Animal Care and Use Committee and was performed in compliance with the guidelines for conducting animal experiments at Kagawa University.

Drugs and solutions

The composition of Hepes-buffered saline solution (HBS) was 10 mM Hepes (pH 7.4), 135 mM NaCl, 5 mM KCl, 1 mM $CaCl_2$, 1 mM $MgCl_2$, 5.5 mM D-glucose. HBS containing 100 mM K^+ was prepared by substituting equimolar NaCl with KCl. The composition of phosphate buffered saline (PBS) was 136.9 mM NaCl, 2.7 mM KCl, 8.1 mM Na_2HPO_4, 1.47 mM KH_2PO_4. The active form of bovine FXIa was purchased from Enzyme Research Laboratories (South Bend, NI, USA). Thrombin (bovine plasma), trypsin (bovine pancreas), thapsigargin, probenecid, 4-amidinophenylmethanesulfonyl fluoride (p-APMSF) and H-89 dihydrochloride hydrate were purchased from Sigma (St. Louis, MO, USA). TFLLR-NH_2, a PAR_1-activating peptide (PAR_1-AP), was synthesized by Eurofins Genomics (Tokyo, Japan). SLIGRL-NH_2, a PAR_2-AP, was purchased from Bachem (Bubendorf, Switzerland). Ionomycin calcium was purchased from LKT Laboratories (St. Paul, MN, USA). Atopaxar was purchased from Axon Medchem (Groningen, Netherlands). YM58483, Pyr3, GF109203X (Gö 6850, bisindolylmaleimide I) and rottlerin were purchased from Tocris (Bristol, UK). Diltiazem was purchased from Focus Biomolecules (Plymouth Meeting, PA, USA). Saracatinib (AZD0830) was purchased from Selleckchem (Houston, TX, USA). LY294002 was purchased from Wako (Osaka, Japan). Fura-2 acetoxymethyl ester (fura-2/AM), was purchased from Dojindo (Kumamoto, Japan).

Cell culture

Rat embryo aorta smooth muscle A7r5 cells (ATCC Cat# CRL-1444, RRID: CVCL_0137) and mouse embryonic fibroblasts (MEFs) were cultured in Dulbecco's modified Eagle medium (DMEM; Sigma) supplemented with 10% fetal bovine serum (Biological Industries, Kibbutz Beit HaEmek, Israel) at 37°C in a humidified 5% CO_2 environment.

Tissue sampling from rats

One 7-week-old male Wistar rat (SLC, Shizuoka, Japan, RRID: RGD_2314928) was euthanized by an intraperitoneal injection of a lethal dose of sodium pentobarbital (50 mg/kg weight) and urethane (1.2 g/kg weight). The brain, aorta, lung, kidney, liver, eye, heart, epididymal adipose tissue, whole blood cells as clots and spleen were isolated and snap-frozen in liquid N_2 for isolation of RNA.

Preparation of MEFs from wild-type and PAR_1 knockout mice

Pregnant female wild-type C57BL/6NCrSlc mice (SLC) and PAR_1 knockout mice (Jackson Laboratory, Bar Harbor, MA, USA; IMSR Cat# JAX:002862, RRID: IMSR_JAX:002862) were euthanized by an intraperitoneal injection of a lethal dose of sodium pentobarbital (50 mg/kg weight) and urethane (1.2 g/kg weight). Mouse fetuses (14-18 days *post coitus*) were removed from the uterus. The fetuses were minced into smaller pieces in sterile PBS using a sterile blade. Minced tissues suspended in DMEM were then filtered through a 300-nm nylon mesh (Sansyo, Tokyo, Japan) using a sterile scraper. The filtrated cells were collected and washed 2 times in DMEM by centrifugation at 800 rpm for 5 min. MEFs obtained from all fetuses of one parent were combined and plated on a 100-mm dish. The MEF culture was occasionally split at an appropriate ratio and maintained under the above-described culture conditions.

Fura-2 fluorometry for measurement of cytosolic Ca^{2+} concentrations

A7r5 cells and MEFs were seeded at 1.5 x 10^5 or 1.0 x 10^5 cells/dish, respectively, on 35-mm dishes and cultured for 3 days. On day 4, the cells were serum-starved overnight, except for the siRNA-treated cells, and then subjected to fura-2 fluorometry on day 5. The cells were loaded with fura-2 by incubating them in DMEM containing 5 μM fura-2/AM and 400 μM probenecid for 60 min under cell culture conditions. After fura-2 loading, the dishes were set on the stage, which was kept at 37°C, and the cells were washed 2-3 times and equilibrated in 1 mL HBS at 37°C. Fluorometry was performed in the presence of 400 μM probenecid to prevent leakage of fura-2 from the cytosol to the extracellular space and a resultant spontaneous gradual increase in fura-2 fluorescence. The changes in the intensities of fura-2 fluorescence at 340 nm (F340) and 380 nm (F380) excitations and their ratio (F340/F380) were monitored using a front-surface fluorometer CAM-230-OF1 (JASCO, Tokyo, Japan), as previously described (5, 13). The fluorescence ratio data were evaluated by either the height in comparison to the base line or the area under curve, as indicated in the Results section and Figure legends and were normalized by the height of peak elevation induced by 50 μM ionomycin. The height and area were measured using the ImageJ 1.42q software program (National Institutes of Health, Bethesda, MD, USA, RRID:SCR_003073).

Isolation of RNA

Total RNA from A7r5 cells and rat tissues were isolated using TRIzol (Life Technologies, Carsbad, CA, USA) and a Tissue Total RNA Extraction Mini Kit (Favorgen Biotech, Ping-Tung, Taiwan, China) according to the manufacturer's instructions. The concentrations of total RNA were estimated by OD_{260}.

Reverse transcription (RT)-PCR

One μg of total RNA was reverse transcribed using oligo dT and random primers in a total volume of 20 µL using a PrimeScript™ RT reagent Kit (Takara, Kusatsu, Japan) according to the manufacturer's instructions. The RT products were diluted 4 times in H_2O. One µL of the diluted cDNA was subjected to a PCR with 10 µL PrimeSTAR Max Premix (Takara), 0.5 µL each primer (concentration of stock solution was 20 µM) and 7 µL distilled water. The PCR products (10 µL) were separated by 1% or 3% agarose gel electrophoresis and stained with 0.5 µg/mL ethidium bromide. The fluorescence image was captured with a Gel Doc EZ Imager (Bio-rad, Tokyo, Japan). The sequences and Tm values of the primers and conditions of the PCR are listed in Table 1. The primers sequences were designed according to the previous reports (14, 31) or by Roche ProbeFinder (https://qpcr.probefinder.com/organism.jsp).

Real-time PCR

The working solution of the real-time PCR was comprised of 7.2 µL SYBR Premix Ex Taq II (Takara), 0.4 µL ROX Reference Dye (Takara), 0.4 µL each primer (concentration of stock solution was 20 µM), 5.1 µL distilled water, and 2 µL of the diluted cDNA. The PCR was performed using an Applied Biosystems ViiA 7 (Life Technologies, Tokyo, Japan). The cycling conditions for PARs were as follows: 10-min initial denaturation at 95°C, followed by a 50-cycle amplification step composed of 5-s denaturation at 95°C and 30-s annealing and extension at 60°C. The cycling conditions for $Ca_V1.2$ were as follows: 60-s initial denaturation at 95°C, followed by a 50-cycle amplification step composed of 30-s denaturation at 95°C, 30-s annealing at 65°C and 30-s extension at 72°C. The cycling conditions for S16, Orai1, Orai2, and Orai3 were as follows: 60-s initial denaturation at 95°C, followed by a 50-cycle amplification step composed of 30-s denaturation at 95°C and 30-s annealing and extension at 60°C. A melting curve analysis was performed after the 50-cycle PCR by increasing the temperature at the rate of 0.05°C/s from the finishing temperature of the PCR to 95°C. The cDNA from rat lung and A7r5 cells un-transfected with siRNA was subjected to 2-fold dilutions 6 times, successively, to prepare the standard samples for PARs and Ca^{2+} channels (Ca_V1.2, Orai1, Orai2, and Orai3), respectively. The Ct values of the fluorescence and the fold dilutions of the standard samples were plotted to obtain a standard curve for each target. The expression levels of mRNAs of S16, PARs and Ca^{2+} channels under different conditions were quantified by fitting the Ct values to the standard curve and then the levels of PARs and Ca^{2+} channels were normalized by the level of S16 mRNA. The primer sequences were listed in Table 1.

Cloning of the rat PAR$_1$ cDNA

The full-length cDNA of the rat PAR$_1$ (accession number: NM_012950.2) was obtained by PCR amplification using cDNA obtained from the lung as a template and the following primers: 5'-TAA GAA AGT AGG CGA CCG CGG T-3' (forward primer designed upstream of the start codon of PAR$_1$) and 5'-GCC ACC CTT TCC CTA AGC TAG TAG CT-3' (reverse primer containing the reverse complement sequences for the stop codon [underlined]). The PCR product was cloned into pT7Blue-T vector (Merck, Darmstadt, Germany) to obtain pT7Blue-PAR$_1$. The sequence of the PAR$_1$ cDNA was determined to have no mutations by a DNA sequencing service (Eurofins Genomics, Tokyo, Japan).

Construction of the expression plasmid of the extracellular region of rat PAR$_1$ flanked by SUMOstar and GST tags.

The cDNA corresponding to the N-terminal extracellular region of rat PAR$_1$ (PAR$_1$E; 22-109 amino acid residues) was amplified by a PCR using the pT7Blue-PAR$_1$ as a template and the following primers: 5'-ATG GTC TCA *AGG T*TC CCG CGT TCC TAT GAG A-3' (forward primer, underline indicates a *Bsa*I recognition site; italic indicates an overhung generated on the (-)-strand upon *Bsa*I digestion) and 5'-AAT CTA GA*T TA*C GTC AGC CAG GGG CTG GT-3' (reverse primer, underline indicates a *Xba*I site; italic indicates the reverse complement sequence of the stop codon). The PCR product of PAR$_1$E was directly sub-cloned into pT7Blue-T vector. The sequence of the PAR$_1$E was confirmed to have no unintended mutations (Eurofins Genomics). The resulting plasmid was digested with *Bsa*I/*Xba*I. The digested fragment containing PAR$_1$E was ligated into the *Bsa*I/*Xba*I site of the pE-SUMOstar plasmid (LifeSensors, Malvern, PA, USA) to obtain pE-SUMOstar-PAR$_1$E. The preliminary experiment indicated that the N-terminal (His)$_6$-SUMOstar-taged PAR$_1$E was susceptible to proteolysis in the homogenate of a host *E. coli*. Thus, glutathione S-transferase from *Schistosoma japonicum* (GST; 2-218 amino acid residues) was further introduced to the C-terminus of (His)$_6$-SUMOstar-taged PAR$_1$E as follows, in order to secure a full-length protein of PAR$_1$E by performing affinity chromatography for the N-terminal (His)$_6$-tag and for the C-terminal GST-tag.

First, site-directed mutagenesis was performed to convert the stop codon of PAR$_1$E to a *Mfe*I site using a PrimeSTAR mutagenesis basal kit (Takara Bio), pE-SUMOstar-PAR$_1$E as a template and the following primers: 5'-TGA CGC AAT TGA GAG GAT CCG AAT TCG AG-3' (forward primer, underlines indicate a *Mfe*I site) and 5'-CCT CTC AAT TGC GTC AGC CAG GGG CTG GT-3' (reverse primer, underlines indicate a *Mfe*I site). The DNA sequencing of the product confirmed the conversion of the stop codon to the *Mfe*I site and showed no unintended mutations. The GST cDNA was amplified by a PCR using a pGEX-4T-1 plasmid (GE Healthcare Japan, Tokyo, Japan) as a template and the following primers: 5'-CTG GCT GAC GCA ATT GTC CCC TAT ACT AGG TTA TTG GAA A-3' (forward primer, underline indicates the sequences corresponding to those upstream of the *Mfe*I site in pE-SUMOstar-PAR$_1$E) and 5'-CGG ATC CTC TCA ATT AAC GCG GAA CCA GAT CCG AT-3' (reverse primer, underline indicates the sequences corresponding to those downstream of the *Mfe*I site in pE-SUMOstar-PAR$_1$E). The PCR product of the GST cDNA was sub-cloned into the *Mfe*I-digested pE-SUMOstar-PAR$_1$E using an In-fusion HD cloning kit (Takara Bio) to obtain pE-SUMOstar-PAR$_1$E-GST. The DNA sequence from the

N-terminal $(His)_6$-SUMOstar through PAR$_1$E to the C-terminal GST tag was determined to have no unintended mutations.

The expression and purification of the SUMOstar- and GST-tagged PAR$_1$E

PAR$_1$E with an N-terminal SUMOstar tag and a C-terminal GST tag was expressed in an *E. coli* strain Rosetta 2 (DE3) pLysS (Merck). The cells harboring pE-SUMOstar-PAR$_1$E-GST were grown in 5 mL of 2x YT medium containing 100 μg/mL of ampicillin (Sigma) and 20 μg/mL of chloramphenicol (Sigma) overnight with rotation at 250 rpm at 37°C and then inoculated to 500 mL of Plusgrow II medium (Nacalai tesque, Kyoto, Japan) containing 100 μg/mL of ampicillin and 20 μg/mL of chloramphenicol. The cells were cultured with rotation at 250 rpm at 37°C for 2 h until the absorbance at 600 nm reached approximately 0.8. The culture was cooled on ice for 5 min and isopropyl β-D-thiogalactopyranoside (Nacalai tesque) was added to the final concentration of 1 mM. The cells were further cultured at 25°C for 8 h with rotation at 250 rpm and then harvested by centrifugation at 10,000×*g* for 10 min and suspended in buffer A (50 mM Hepes-NaOH, pH 7.4, 200 mM NaCl) supplemented with 0.1 mM EDTA and a protease inhibitor cocktail tablet (cOmplete Ultra; Roche Diagnostics, Tokyo, Japan). The cells were then broken on ice by sonication for 12 min with 3-min intervals on a SONIFER 250D-Advanced sonicator (Branson Ultrasonics, Danbury, CT, USA). The unbroken cells, inclusion bodies and membrane fractions were removed by ultracentrifugation at 184,000×*g* for 60 min. The supernatant was applied onto a 5-mL Ni-sepharose column (HisTrap HP; GE Healthcare) equilibrated with buffer A supplemented with 0.1 mM EDTA and 1 mM phenylmethylsulfonyl fluoride (PMSF). The column was washed with 10-column volumes of buffer A supplemented with 0.1 mM EDTA, 1 mM PMSF and 10 mM imidazole. The SUMOstar-PAR$_1$-GST protein was then eluted by a linear gradient of 10 to 250 mM imidazole in 20-column volumes of buffer A supplemented with 0.1 mM EDTA and 1 mM PMSF. A portion of 2-mL fraction was subjected to

SDS-polyacrylamide (10%) gel electrophoresis prepared by WIDE RANGE buffer (Nacalai tesque) and stained with CBB Stain One Super (Nacalai tesque). Fractions with less degradation were pooled and concentrated by ultrafiltration on VivaSpin Turbo 50 kDa MWCO (Sartorius Stedim Biotech, Goettingen, Germany) and desalted with a desalting column EconoPac 10DG (Bio-Rad Laboratories, Hercules, CA, USA) equilibrated with buffer A supplemented with 10%(w/v) glycerol. After adding dithiothreitol (DTT) at a final concentration of 10 mM, the desalted fraction was applied onto a 2-mL glutathione sepharose column GSTrap 4B (GE Healthcare) equilibrated with buffer A supplemented with 10% (w/v) glycerol and 10 mM DTT. The column was washed with 10-column volumes of the same buffer and the target protein was eluted as a single peak in buffer A supplemented with 10% (w/v) glycerol, 10 mM DTT and 15 mM glutathione. The eluates were pooled and concentrated by ultrafiltration, and then desalted with a desalting column with buffer A supplemented with 10% (w/v) glycerol. The yield of SUMOstar-PAR$_1$E-GST was > 20 mg/500 mL culture. The purity of the final preparation was > 90%, as determined by the density of the 53 kDa band on a SDS-polyacrylamide (10%) gel stained with CBB Stain One Super. The desalted specimen was aliquoted, quickly frozen in liquid nitrogen, and stored at -80°C until use.

In vitro digestion of PAR$_1$E by thrombin and FXIa

The SUMOstar-PAR$_1$E-GST protein was diluted with a buffer consisting of 50 mM Hepes-NaOH (pH 7.4), 200 mM NaCl and 10% (w/v) glycerol at a final concentration of 10 μM (0.49 mg/mL). The protein solution was then incubated for 5 min at 25°C. After incubation, proteolytic digestion was started by adding thrombin and FXIa at a final concentration of 1 unit/mL (approximately 10 nM) and 300 nM, respectively. At each time point, a portion of the reaction mixture was made 50 μM p-APMSF, a serine protease inhibitor, and mixed with one volume of 2x Laemmli sample loading buffer to stop the proteolytic reaction. The digests were subjected to SDS-polyacrylamide (10%) gel electrophoresis and analyzed by staining with CBB Stain One Super.

Protein sequencing

The digests of the recombinant SUMOstar-PAR$_1$E-GST obtained with 100-min treatment with 1 unit/mL thrombin and 300 nM FXIa were subjected to SDS-polyacrylamide (10%) gel electrophoresis and transferred onto the polyvinylidene fluoride membrane. The membrane was stained with 0.025% CBB R-250 for 5 min, and the part of the membrane that contains the 33.6-kDa fragment was cut out. The membrane pieces were thoroughly washed with distilled water and then 50% methanol, dried under vacuum, and then subjected to protein sequencing on Protein Sequencer Procise 492 (Applied Biosystems, Waltham, MA, USA). The first four amino acids residues of the fragment were determined.

Transfection of siRNA

A7r5 cells were seeded at 8 x10^4 cells/dish on 35-mm dishes. On the following day, the cells were transfected with siRNA using Lipofectamine RNAiMAX (Life Technologies, Carsbad, CA, USA) according to the manufacturer's instruction. In brief, 4 μL Lipofectamine RNAiMAX was mixed with 100 μL Opti MEM and incubated for 5 min at room temperature, followed by addition of siRNA duplexes and incubation for further 5 min at room temperature. Then, the mixture was added to the culture media containing 10% fetal bovine serum. The final concentration of siRNAs against Ca$_V$1.2, Orai1, Orai2, and Orai3 and MISSION siRNA Universal Negative Control (Sigma) was 10 nM. The cells were then subjected to fura-2 fluorometry and total RNA isolation 3 days after transfection. The knockdown efficiency was evaluated by a real-time PCR, as described above. The siRNA sequences are listed in Table 2.

Wound healing assay

Cells were seeded on 35-mm dishes, which were divided into 4 sectors (Greiner Bio-one, Kremsmünster, Austria), at 3 x10^4 cells/sector and cultured for 3 days until confluence. The cells were serum-starved for 11 h, and then the scratch wounds were applied with a 200-μL pipette tip, followed by washing in DMEM and the initiation of drug treatment in DMEM. The dishes were set on the stage of a BZ-9000 All-in-One fluorescence microscope (Keyence, Osaka, Japan) equipped with an on-stage chamber providing routine culture conditions (37°C, 5% CO_2). The phase contrast microscopic images were consecutively captured from the fixed three areas for each sector at a 30-min interval for 24 h. On each image, both edges of the wound were outlined by two parallel lines and the distance between two lines were measured as a width of wound at each time point, using a BZ-II analysis application software (Keyence, RRID: SCR_016348). The wound widths were plotted as a function of the time, and the data obtained with the first 10 h were fitted to the linear regression ($r^2 > 0.91$). The migration rate for the first 10 h was estimated by a slop of the regression line. The preliminary analysis of the cell cycle progression after replating the cells at confluence with propidium iodide staining indicated that a significant degree of the S phase entry was not observed until 15 h after replating, even in the presence of 10% serum (Data no show). Thus, the involvement of cell proliferation in wound healing event could be mostly omitted by analyzing the events during the first 10 h.

Statistics

The data are expresses as the mean ± SD of the indicated number of independent experiments. An analysis of variance (ANOVA) followed by Dunnett's post-hoc test was used for comparisons with the controls, and ANOVA followed by the Bonferroni-Dunn test was used for multiple comparisons. All statistical analyses were performed using the StatView software program (ver. 5, SAS Institute, Cary, NC, USA). P values of < 0.05 were considered to indicate statistical significance.

Results

FXIa induces Ca^{2+} release and Ca^{2+} influx in A7r5 cells.

The removal of extracellular Ca^{2+} and addition of 2 mM EGTA to the bathing solution caused a decrease in the resting level of the cytosolic Ca^{2+} concentrations ($[Ca^{2+}]_i$) in A7r5 cells (all traces in Figure 1). The subsequent replenishment of 2 mM extracellular Ca^{2+} with no stimulation increased $[Ca^{2+}]_i$ to a level that was slightly higher than the initial level seen in the presence of 1 mM extracellular Ca^{2+} (Figure 1A). In the absence of extracellular Ca^{2+}, 300 nM FXIa induced a significant but small transient elevation of $[Ca^{2+}]_i$ (0.014 ± 0.007 A.U.) (Figure 1B). This transient Ca^{2+} response is attributable to the release of Ca^{2+} from the intracellular store sites. The subsequent replenishment of extracellular Ca^{2+} induced a sustained elevation of $[Ca^{2+}]_i$ (0.450 ± 0.047 A.U.) (Figure 1B). This sustained response is attributable to extracellular Ca^{2+} influx. At concentration ≤ 100 nM, FXIa significantly induced Ca^{2+} influx in a concentration-dependent manner, but without any appreciable Ca^{2+} release (Figure 1B). Thapsigargin, an inhibitor of endoplasmic Ca^{2+} ATPase, concomitantly induced Ca^{2+} release and Ca^{2+} influx, which reached the maximal levels of 0.418 ± 0.074 and 0.645 ± 0.019 (A.U.), respectively, at 1 μM (Figure 1C). Thrombin, Trypsin, TFLLR-NH_2 (PAR_1-activating peptide) and SLIGRL-NH_2 (PAR_2-activating peptide) induced both Ca^{2+} release and Ca^{2+} influx in a concentration-dependent manner (Figures 1D, 1E, 1F and 1G, respectively).

FXIa induces Ca^{2+} responses via PAR_1

A real-time PCR demonstrated the mRNA expression of PAR_1, PAR_2 and PAR_3 in A7r5 cells, while the level of PAR_2 was the greatest and that of PAR_3 was residual (Figure 2A). No appreciable expression of PAR_4 was observed. A PAR_1 antagonist, atopaxar, inhibited both the Ca^{2+} release and Ca^{2+} influx induced by 30 μM TFLLR-NH_2 in a concentration-dependent manner (Figure 2B). Atopaxar exhibited a complete inhibition at 1 μM.

Treatment with 1 μM atopaxar also abolished the FXIa-induced Ca^{2+} release and Ca^{2+} influx (Figure 2C). In contrast, both Ca^{2+} release and Ca^{2+} influx induced by 30 μM SLIGRL-NH_2 were resistant to 1 μM atopaxar. Furthermore, the Ca^{2+} influx induced by 1 μM thapsigargin was also resistant to 1 μM atopaxar. The Ca^{2+} release induced by 1 μM thapsigargin was partly but significantly inhibited by 1 μM atopaxar (Figure 2C). The reason for this inhibition is unclear.

The proteolytic activation is a canonical mechanism of the activation of PARs (40, 45). When thrombin or FXIa was pre-incubated with a serine protease inhibitor, p-APMSF, in a concentrated small volume for 15 min and then applied to the cells, both thrombin and FXIa lost their activity to generate a Ca^{2+} response (Figure 2D). In contrast, the activity of TFLLR-NH_2 (a peptide agonist of PAR_1) to generate a Ca^{2+} response was resistant to p-APMSF pretreatment (Figure 2D).

In wild-type MEFs, 30 μM TFLLR-NH_2 and 1 unit/mL thrombin induced a transient elevation of $[Ca^{2+}]_i$ in the absence of extracellular Ca^{2+} but did not induce an appreciable Ca^{2+} response after replenishing the extracellular Ca^{2+} (Figure 3). FXIa at a concentration of 300 nM also induced a small but consistent transient elevation in $[Ca^{2+}]_i$ in the absence of extracellular Ca^{2+} (Figure 3). All of these transient Ca^{2+} responses due to Ca^{2+} release that were seen with TFLLR-NH_2, thrombin and FXIa were abolished in the $PAR_1^{-/-}$ MEFs. In contrast, the Ca^{2+} response induced by 1 μM thapsigargin was resistant to PAR_1 gene knockout (Figure 3).

The ability of FXIa to cleave the extracellular region of PAR_1 (PAR_1E) was examined by an *in vitro* digestion assay using a recombinant protein containing SUMOstar and GST-tagged PAR_1E (Figure 4A). Both 1 unit/mL thrombin and 300 nM FXIa yielded a similar pattern of digestion (Figure 4B). The digests exhibited the expected molecular size when cleaved at the established thrombin site. However, the rate and efficacy of digestion by thrombin were much greater than that seen with FXIa (Figure 4). Thrombin completely cleaved the protein within 5 min, while FXIa did not show complete digestion, even after 100 min. The first four N-terminal amino acids of the PAR_1E-GST fragment obtained with digestion by both thrombin and FXIa were SFFL (Figure 4C).

FXIa induces Ca^{2+} influx via $Ca_V1.2$

The mechanism of Ca^{2+} influx was further investigated using 100 nM FXIa, as this concentration predominantly induced Ca^{2+} influx (Figure 1). First, the effects of the three following pharmacological inhibitors of Ca^{2+} influx channels on the FXIa-induced Ca^{2+} influx were examined: YM58483, a blocker of the store-operated Ca^{2+} entry (SOCE), Pyr3, an inhibitor of the transient receptor potential canonical channel 3 (TRPC3), and diltiazem, a blocker of the L-type Ca^{2+} channel. The peak and plateau (8 min after stimulation) levels of $[Ca^{2+}]_i$ elevation induced by 100 mM K^+-depolarization were inhibited by 10-min pretreatment with diltiazem in a concentration-dependent manner (Figure 5A). Complete inhibition was observed with 10 μM diltiazem. Pretreatment with 3 μM YM58483 had no significant effect on the 100 mM K^+-induced $[Ca^{2+}]_i$ elevation. Pretreatment with 3 μM Pyr3 slightly inhibited the 100 mM K^+-induced $[Ca^{2+}]_i$ elevation at plateau. In contrast, the sustained level of $[Ca^{2+}]_i$ elevation at 8 min after Ca^{2+} replenishment during stimulation with 1 μM thapsigargin was inhibited by YM58483 and Pyr3 in a concentration-dependent manner, when these inhibitors were applied at the time of Ca^{2+} replenishment (Figure 5B). The complete inhibition of the thapsigargin-induced Ca^{2+} influx was obtained at 3 μM for both inhibitors. On the other hand, 10 μM diltiazem had no significant effect on the thapsigargin-induced Ca^{2+} influx (Figure 5B). The above observations demonstrated that the three inhibitors hold some specificity regarding the different mechanisms of Ca^{2+} influx. The Ca^{2+} influx induced by 100 nM FXIa, 1 unit/mL thrombin, and 30 μM TFLLR-NH_2 was, in each case, abolished by 10 mM diltiazem, whereas it was largely resistant to 3 μM YM58483 and 3 μM Pyr3 (Figure 5C).

The observations with the pharmacological inhibitors were corroborated by the experiment with the siRNA-mediated knock-down of the expression of the relevant Ca^{2+} channels. First, the mRNA expression of relevant Ca^{2+} influx channels, including TRPC3, Ca$_V$1.2, Ca$_V$1.3 and Orai1-3, in A7r5 cells was examined by RT-PCRs (Figure 6). According to the results of the preliminary experiments performed with various tissues, brain, aorta, lung and kidney tissues were selected as a positive control for each of Ca^{2+} influx channels that were examined. A7r5 cells were found to express Ca$_V$1.2, Orai1-3, but not TRPC3 and Ca$_V$1.3 (Figure 6).

The transfection of 10 nM siRNA against Ca$_V$1.2, Orai1, Orai2, and Orai3 caused a specific knock-down of the expression of the target channels (Figure 7A). The peak and plateau response of the 100 mM K^+-induced $[Ca^{2+}]_i$ elevation was partly but significantly inhibited by the knock-down of Ca$_V$1.2, while they were totally resistant to the knock-down of Orai1-3 (Figure 7B). The Ca^{2+} influx induced by 1 μM thapsigargin was partly but significantly inhibited by the knock-down of Orai1, but not Ca$_V$1.2, Orai2 or Orai3. The thapsigargin-induced Ca^{2+} release was resistant to the knock-down of any target. The Ca^{2+} influx induced by 1 unit/mL thrombin and 100 nM FXIa was partly but significantly inhibited by the knock-down of Ca$_V$1.2, but not Orai1-3. The findings with the pharmacological inhibitors and the siRNA-mediated knock-down of Ca^{2+} channels consistently suggest the involvement of the L-type Ca^{2+} channel Ca$_V$1.2 in the FXIa-induced Ca^{2+} influx.

The FXIa-induced activation of Ca^{2+} influx involves Protein Kinase Cδ

Ca$_V$1.2 has been shown to be activated by the phosphorylation catalyzed by protein kinase A (PKA) (3, 6, 23), protein kinase C (PKC) (44), Ca^{2+}/calmodulin-dependent protein kinase II (CaMKII) (19) or src family tyrosine kinase (11) and by the interaction with phosphatidyl-inositol trisphosphate, a product of phosphatidyl-inositol 3-kinase (PI3-kinase) (18). Thus, the effects of H-89 (PKA inhibitor), GF109203X (Pan-PKC inhibitor), rottlerin

(PKCδ inhibitor), KN-93 (CaMKII inhibitor), LY294002 (PI3-kinase inhibitor), and AZD0530 (saracatinib; src family tyrosine kinase inhibitor) on the FXIa-induced Ca^{2+} response were examined (Figure 8).

First, we examined the effects of these inhibitors on the 100 mM K^+-induced Ca^{2+} influx (Figures 8A and 8B). The inhibitors were applied 10 min prior to and during 100 mM K^+ depolarization. The peak and plateau levels of the 100 mM K^+-induced $[Ca^{2+}]_i$ elevation were substantially inhibited by 10 μM KN-93. This observation precluded the further discussion on the involvement of CaMKII in the FXIa-induced Ca^{2+} influx. In contrast, only a small but significant inhibition was observed under some conditions; 3 μM rottlerin vs. peak and plateau levels, 10 μM H89 vs. plateau level and 10 μM LY294002 vs. peak and plateau levels (Figures 8A and 8B). These inhibitors are thus considered to be useful for investigating the involvement of their target kinases in the FXIa-induced Ca^{2+} influx.

During the Ca^{2+} add-back protocol used to observe the agonist-induced Ca^{2+} response, the kinase inhibitors were applied at the time of removal of the extracellular Ca^{2+}. None of the inhibitors exerted a significant inhibitory effect on the Ca^{2+} release induced by 1 unit/mL thrombin and 30 μM TFLLR-NH_2 (Figures 8A and 8B). The Ca^{2+} influx induced by thrombin, TFLLR-NH_2 and 100 nM FXIa was substantially inhibited by 1 μM GF109203X, 3 μM rottlerin and 10 μM KN-93 (Figures 8A, 8B and 8C). The Ca^{2+} influx induced by FXIa was also inhibited by 1 μM rottlerin (Figure 8C). The Ca^{2+} influx induced by TFLLR-NH_2 and FXIa was also significantly inhibited by 10 μM H-89. However, this inhibition appeared to be smaller than that seen with 3 μM GF109203X, especially in the case of FXIa (Figure 8A and 8C).

The functional role of FXIa-induced Ca^{2+} signaling in cell migration

The functional role of FXIa-induced Ca^{2+} signaling in cell migration was investigated with a wound healing assay (Figure 9). Confluent culture was subjected to scratch wound (585.1 ±

67.1 μm of all 80 wounds) and the migration of cells to the wound was observed in the absence of serum. In the absence of any stimulation, the wound closed at 12.54 ± 2.83 μm/h during the first 10 h after scratching but did not reach complete wound closure within 24 h. In the presence of 300 nM FXIa, the migration rate was significantly accelerated by 2.46 ± 0.32 fold (Figures 9A and 9B) and the wound was completely closed by 24 h. The FXIa-induced acceleration was partly but significantly inhibited by 1 μM atopaxar and 10 μM diltiazem (Figure 9B). The combination of 1 μM atopaxar and 10 μM diltiazem did not cause greater inhibition than that seen with either atopaxar or diltiazem alone (Figure 9B). Diltiazem, but not atopaxar, also decreased the rate of control migration (Figure 9B). Treatment with 1 unit/mL thrombin, 30 μM TFLLR-NH_2 or 30 μM SLIGRL-NH_2 had no significant effect on the cell migration rate (Figure 9B).

Discussion

The present study demonstrates for the first time that FXIa induces cellular effects in vascular smooth muscle cells. FXIa mainly elicited intracellular Ca^{2+} signaling by the PAR_1 and $Ca_V1.2$-mediated Ca^{2+} influx in A7r5 cells. Functionally, FXIa accelerated cell migration in a manner that was partly dependent on PAR_1 and Ca^{2+} influx. The findings of the present study therefore suggest a novel role of FXIa as a regulator of the vascular smooth muscle functions beyond its well-established role as a coagulation factor of the intrinsic pathway. FXIa has been suggested to be involved in the pathogenesis of atherosclerosis based on the observation that the genetic knockout of FXI protected the development of atherosclerosis induced by a high-fat diet in mice (33). The direct vascular effect of FXIa that was observed in the present study may contribute, in part, to its role in atherogenesis.

The real-time PCR showed the mRNA expression of PAR_1, PAR_2 and PAR_3 in A7r5 cells, with PAR_2 being the highest, PAR_1 being the second highest and PAR_3 being residual. The observations with a PAR_1 antagonist, atopaxar, and $PAR_1^{-/-}$ MEFs support the major involvement of PAR_1 in mediating the Ca^{2+} signal elicited by FXIa. Atopaxar showed some specificity in its inhibition of the Ca^{2+} signaling induced by TFLLR-NH_2, a PAR_1-AP, but not that induced by SLIGRL-NH_2, a PAR_2-AP. Atopaxar partially inhibited the thapsigargin-activated Ca^{2+} release (Figure 2). Thapsigargin is an inhibitor of sarco-endoplasmic reticulum Ca^{2+} ATPase (30). In the absence of extracellular Ca^{2+}, thapsigargin induces a passive Ca^{2+} release from the intracellular store sites following the blockade of Ca^{2+} uptake into the store sites. The inhibition of the thapsigargin-induced Ca^{2+} release by atopaxar is thus considered to be attributed to non-specific inhibition of Ca^{2+} release mechanism, such as inositol-trisphosphate receptor, ryanodine receptor or some Ca^{2+} leak channels. The similar mechanism might be involved in the atopaxar inhibition of the FXIa- and PAR_1-AP-induced Ca^{2+} release. However, this is unlikely as atopaxar had no effect on the Ca^{2+} release induced by a receptor agonist, PAR_2-AP. Although the reason for the inhibition of the thapsigargin-induced Ca^{2+} release by atopaxar remains unclear, the observations with atopaxar plausibly support the contribution of PAR_1 to the Ca^{2+} response induced by FXIa.

In the wild-type MEF, FXIa, thrombin and TFLLR-NH_2 all induced the release of Ca^{2+} from the intracellular store sites, with no appreciable influx of extracellular Ca^{2+}. The mechanisms underlying the PAR_1-mediated Ca^{2+} signaling in MEFs therefore appear to be different from those in A7r5 cells. Nevertheless, the specific abolishment of the Ca^{2+} signaling effect of FXIa, thrombin and TFLLR-NH_2 in $PAR_1^{-/-}$ MEFs suggests that PAR_1 plays a major role in mediating the effect of FXIa. In contrast, the thapsigargin-induced Ca^{2+} release and Ca^{2+} influx were both resistant to PAR_1 gene knockout.

In a canonical tethered-ligand mechanism, PAR_1 is activated by the proteolytic cleavage of the extracellular region (45). The Ca^{2+} signaling effect of FXIa was abolished by pretreatment with a proteinase inhibitor. The *in vitro* digestion assay indeed indicates the ability of FXIa to cleave the extracellular region of PAR_1, and in a similar pattern to that seen with thrombin digestion. Furthermore, the protein sequencing of the digest indicated that FXIa cleaved the canonical thrombin site (R45/S46) of the rat PAR_1 (35). These observations suggest that FXIa activates PAR_1 in a similar manner to that which occurs during thrombin stimulation.

Extracellular Ca^{2+} influx plays a major role in the FXIa-induced Ca^{2+} signaling in A7r5 cells. The mechanism underlying the FXIa-induced Ca^{2+} influx was therefore further investigated using 100 nM FXIa, because this concentration specifically activated Ca^{2+} influx without significantly activating Ca^{2+} release. The effects of the pharmacological inhibitors of several Ca^{2+} influx mechanisms and the siRNA-mediated knockdown of channel proteins consistently suggested the major role of a voltage-dependent, L-type Ca^{2+} channel, $Ca_V1.2$. The specific knockdown of the expression of the target genes was confirmed by a real-time PCR. However, the efficacy of knockdown was approximately 35%-40% at 10 nM siRNA.

The partial knockdown of the target genes is consistent with the partial inhibition of the Ca^{2+} influx. The higher concentrations of siRNA suppressed the expression of non-target proteins (data not shown). Therefore, no concentrations higher than 10 nM were used in the present study. Only a few studies reported the types of Ca^{2+} channel activated by PAR_1. In rat duodenal smooth muscle, the PAR_1-mediated contraction was inhibited by nifedipine and SK&F96365, suggesting the involvement of the L-type Ca^{2+} channel (16). In nociceptive neurons, TRPV1 has been shown to be activated by PAR_1 and PAR_4 (39).

The G protein-coupled receptors activate $Ca_V1.2$ by a mechanism that is dependent on protein phosphorylation. The possible involvement of the phosphorylation-dependent activation of $Ca_V1.2$ by FXIa as well as some identity of the protein kinase involved were investigated using pharmacological inhibitors of several kinases. As a result, the substantial suppression of the Ca^{2+} influx induced by FXIa, thrombin and TFLLR-NH_2 by two PKC inhibitors, GF109203X and rottlerin, was taken as a significant observation. According to the reported isoform specificity of GF109203X (PKCα, βI, βII, γ, δ, ε with IC_{50} values of 20-200 nM in cell-free assays (22, 36)) and rottlerin (PKCδ with IC_{50} values of 3-6 μM in cell-free assays (10)), PKCδ is suggested to play a critical role in the activation of $Ca_V1.2$ by FXIa as well as thrombin and TFLLR-NH_2 in A7r5 cells.

The functional role of the FXIa-induced Ca^{2+} signaling in accelerating cell migration was investigated by the wound healing assay. The preliminary analysis of cell cycle progression with propidium iodide staining indicated that A7r5 cells restart DNA replication as early as 15 h after replating the cells at confluence (Data not shown). By analyzing the rate of wound healing during the first 10 h after applying the wound, the possible contribution of cell proliferation to the wound healing process was eliminated. FXIa was found to accelerate the cell migration in a manner that was partly dependent on PAR_1 and L-type Ca channel. The blockade of the L-type Ca^{2+} channels is reported to decelerate cell migration (17, 21, 26). In migrating cells, calcium plays a multifunctional role in directional sensing, cytoskeleton redistribution, traction force generation, and relocation of focal adhesion (41). In the present study, diltiazem partially inhibited the basal cell migration seen without FXIa stimulation. It is noteworthy that the combination of atopaxar and diltiazem failed to inhibit the FXIa-induced acceleration of cell migration to a greater extent than was observed with a single treatment with either atopaxar or diltiazem. This observation indicates that PAR_1 and $Ca_V1.2$ contribute to the FXIa-induced acceleration of cell migration. However, some mechanisms independent of a PAR_1/$Ca_V1.2$ axis are also suggested to contribute to the acceleration of cell migration by FXIa. Such mechanisms still remain to be elucidated.

Thrombin and TFLLR-NH_2 mainly induced Ca^{2+} signaling via Ca^{2+} influx, as in the case of FXIa. Furthermore, both FXIa and thrombin cleaved the same site of PAR_1 to activate it. However, thrombin and TFLLR-NH_2 had no significant effect on cell migration. The reason for this discrepancy remains unaddressed. Although FXIa cleaved PAR_1 at the same site as that of thrombin, the kinetics of digestion by FXIa was significantly slower than that of thrombin. The slower kinetics seen with FXIa may be preferable for inducing a long-term cellular effect, such as cell migration. However, the cleavage kinetics still remain to be examined with the full-length PAR_1 as well as in a cellular context. Alternatively, the involvement of subtypes of PAR other than PAR_1 may differ between FXIa and thrombin. Such difference may underlie the difference in the effect on cell migration, as some mechanisms independent of a PAR_1/$Ca_V1.2$ axis are suggested to contribute to the acceleration of cell migration by FXIa. Thrombin is known to activate PAR_1, PAR_3 and PAR_4 (12). The effect of FXIa on the subtypes of PAR other than PAR_1 still remain to be investigated.

FXI circulates in plasma at a concentration of ~30 nM (15–45 nM) almost entirely as a non-covalent complex with HK (24). The FXIa concentration in plasma in healthy individuals and patients with acute myocardial infarction or burn injury reaches as high as several pM (20, 34). These concentrations are apparently lower than those required to induce the cellular effects observed in the present study. When the circulating 30 nM FXI is fully activated at the coagulation site, then the local concentration of FXIa may reach a level that is sufficient to induce cellular effects. FXI lacks the Gla domain that facilitates the binding of vitamin K-dependent coagulation factors to phospholipid surfaces, such as the membranes of activated platelets or damaged tissues (24). Instead, HK facilitates FXI binding to the surface of platelets (1). HK may also facilitate FXI binding to the membrane of vascular smooth muscle cells, thereby further increasing the local concentration of FXI to a level that is sufficient to induce cellular effects.

In conclusion, the present study demonstrated the novel function of FXIa as a regulator of vascular smooth muscle. FXIa induces Ca^{2+} signaling mainly due to the PAR_1 and $Ca_V1.2$-mediated Ca^{2+} influx. The activation of $Ca_V1.2$ by FXIa is suggested to depend on PKC, and PKCδ is a plausible isoform involved in the activation of $Ca_V1.2$. Functionally, FXIa causes the acceleration of cell migration, partly due to PAR_1/$Ca_V1.2$-mediated Ca^{2+} signaling. The results of studies with the FXIa-knockout mice suggest that FXI contributes to the pathogenesis of atherosclerosis. Thus, the findings of the present study shed some light on the underlying mechanism. The direct cellular effects of FXIa in vascular smooth muscle cells may, in part, contribute to atherogenesis.

Acknowledgments

We thank Dr. Brian Quinn (Kyushu University, Fukuoka, Japan) for his linguistic assistance.

Grants

This study was supported in part by JSPS KAKENHI (Grant No. 16K09518).

Disclosures

All authors have no conflict of interest.

References

1. **Baglia FA, Gailani D, Lopez JA, Walsh PN**. Identification of a binding site for glycoprotein Ibalpha in the Apple 3 domain of factor XI. *J Biol Chem* 279: 45470-45476, 2004.
2. **Coughlin SR**. Thrombin signalling and protease-activated receptors. *Nature* 407: 258-264, 2000.
3. **De Jongh KS, Murphy BJ, Colvin AA, Hell JW, Takahashi M, Catterall WA**. Specific phosphorylation of a site in the full-length form of the α1 subunit of the cardiac L-type calcium channel by adenosine 3',5'-cyclic monophosphate-dependent protein kinase. *Biochemistry* 35: 10392-10402, 1996.
4. **Emsley J, McEwan PA, Gailani D**. Structure and function of factor XI. *Blood* 115: 2569-2577, 2010.
5. **Eto W, Hirano K, Hirano M, Nishimura J, Kanaide H**. Intracellular alkalinization induces Ca^{2+} influx via non-voltage-operated Ca^{2+} channels in rat aortic smooth muscle cells. *Cell Calcium* 34: 477-484, 2003.
6. **Fuller MD, Emrick MA, Sadilek M, Scheuer T, Catterall WA**. Molecular mechanism of calcium channel regulation in the fight-or-flight response. *Sci Signal* 3: ra70, 2010.
7. **Gailani D, Broze GJ, Jr.** Factor XI activation in a revised model of blood coagulation. *Science* 253: 909-912, 1991.
8. **Gailani D, Gruber A**. Factor XI as a Therapeutic Target. *Arterioscler Thromb Vasc Biol* 36: 1316-1322, 2016.
9. **Gailani D, Lasky NM, Broze GJ, Jr.** A murine model of factor XI deficiency. *Blood Coagul Fibrinolysis* 8: 134-144, 1997.
10. **Gschwendt M, Muller HJ, Kielbassa K, Zang R, Kittstein W, Rincke G, Marks F.**

Rottlerin, a novel protein kinase inhibitor. *Biochem Biophys Res Commun* 199: 93-98, 1994.

11. **Gui P, Wu X, Ling S, Stotz SC, Winkfein RJ, Wilson E, Davis GE, Braun AP, Zamponi GW, Davis MJ.** Integrin receptor activation triggers converging regulation of $Ca_V1.2$ calcium channels by c-Src and protein kinase A pathways. *J Biol Chem* 281: 14015-14025, 2006.
12. **Hirano K.** The roles of proteinase-activated receptors in the vascular physiology and pathophysiology. *Arterioscler Thromb Vasc Biol* 27: 27-36, 2007.
13. **Hirano K, Nomoto N, Hirano M, Momota F, Hanada A, Kanaide H.** Distinct Ca^{2+} requirement for NO production between proteinase-activated receptor 1 and 4 (PAR_1 and PAR_4) in vascular endothelial cells. *J Pharmacol Exp Ther* 322: 668-677, 2007.
14. **Ihara E, Hirano K, Hirano M, Nishimura J, Nawata H, Kanaide H.** Mechanism of down-regulation of L-type Ca^{2+} channel in the proliferating smooth muscle cells of rat aorta. *J Cell Biochem* 87: 242-251, 2002.
15. **Itakura A, Verbout NG, Phillips KG, Insall RH, Gailani D, Tucker EI, Gruber A, McCarty OJ.** Activated factor XI inhibits chemotaxis of polymorphonuclear leukocytes. *J Leukoc Biol* 90: 923-927, 2011.
16. **Kawabata A, Kuroda R, Kuroki N, Nishikawa H, Kawai K, Araki H.** Characterization of the protease-activated receptor-1-mediated contraction and relaxation in the rat duodenal smooth muscle. *Life Sci* 67: 2521-2530, 2000.
17. **Kim JM, Lee M, Kim N, Heo WD.** Optogenetic toolkit reveals the role of Ca^{2+} sparklets in coordinated cell migration. *Proc Natl Acad Sci U S A* 113: 5952-5957, 2016.
18. **Le Blanc C, Mironneau C, Barbot C, Henaff M, Bondeva T, Wetzker R, Macrez N.** Regulation of vascular L-type Ca^{2+} channels by phosphatidylinositol 3,4,5-trisphosphate. *Circ Res* 95: 300-307, 2004.
19. **Lee TS, Karl R, Moosmang S, Lenhardt P, Klugbauer N, Hofmann F, Kleppisch T,**

Welling A. Calmodulin kinase II is involved in voltage-dependent facilitation of the L-type $Ca_V1.2$ calcium channel: Identification of the phosphorylation sites. *J Biol Chem* 281: 25560-25567, 2006.

20. **Loeffen R, van Oerle R, de Groot PG, Waltenberger J, Crijns HJ, Spronk HM, ten Cate H**. Increased factor XIa levels in patients with a first acute myocardial infarction: the introduction of a new thrombin generation based factor XIa assay. *Thromb Res* 134: 1328-1334, 2014.

21. **Lohr C, Heil JE, Deitmer JW**. Blockage of voltage-gated calcium signaling impairs migration of glial cells in vivo. *Glia* 50: 198-211, 2005.

22. **Martiny-Baron G, Kazanietz MG, Mischak H, Blumberg PM, Kochs G, Hug H, Marme D, Schachtele C**. Selective inhibition of protein kinase C isozymes by the indolocarbazole Gö 6976. *J Biol Chem* 268: 9194-9197, 1993.

23. **Minobe E, Maeda S, Xu J, Hao L, Kameyama A, Kameyama M**. A new phosphorylation site in cardiac L-type Ca^{2+} channels ($Ca_V1.2$) responsible for its cAMP-mediated modulation. *Am J Physiol Cell Physiol* 307: C999-C1009, 2014.

24. **Mohammed BM, Matafonov A, Ivanov I, Sun MF, Cheng Q, Dickeson SK, Li C, Sun D, Verhamme IM, Emsley J, Gailani D**. An update on factor XI structure and function. *Thromb Res* 161: 94-105, 2018.

25. **Naito K, Fujikawa K**. Activation of human blood coagulation factor XI independent of factor XII. Factor XI is activated by thrombin and factor XIa in the presence of negatively charged surfaces. *J Biol Chem* 266: 7353-7358, 1991.

26. **Paez PM, Fulton DJ, Spreur V, Handley V, Campagnoni AT**. Multiple kinase pathways regulate voltage-dependent Ca^{2+} influx and migration in oligodendrocyte precursor cells. *J Neurosci* 30: 6422-6433, 2010.

27. **Renne T, Pozgajova M, Gruner S, Schuh K, Pauer HU, Burfeind P, Gailani D, Nieswandt B**. Defective thrombus formation in mice lacking coagulation factor XII. *J*

Exp Med 202: 271-281, 2005.

28. **Rosen ED, Gailani D, Castellino FJ**. FXI is essential for thrombus formation following $FeCl_3$-induced injury of the carotid artery in the mouse. *Thromb Haemost* 87: 774-776, 2002.

29. **Ruf W**. Proteases, Protease-Activated Receptors, and Atherosclerosis. *Arterioscler Thromb Vasc Biol* 38: 1252-1254, 2018.

30. **Sabala P, Czarny M, Woronczak JP, Baranska J**. Thapsigargin: potent inhibitor of Ca^{2+} transport ATP-ases of endoplasmic and sarcoplasmic reticulum. *Acta Biochim Pol* 40: 309-319, 1993.

31. **Sabourin J, Bartoli F, Antigny F, Gomez AM, Benitah JP**. Transient Receptor Potential Canonical (TRPC)/Orai1-dependent Store-operated Ca^{2+} Channels: NEW TARGETS OF ALDOSTERONE IN CARDIOMYOCYTES. *J Biol Chem* 291: 13394-13409, 2016.

32. **Seasholtz TM, Majumdar M, Kaplan DD, Brown JH**. Rho and Rho kinase mediate thrombin-stimulated vascular smooth muscle cell DNA synthesis and migration. *Circ Res* 84: 1186-1193, 1999.

33. **Shnerb Ganor R, Harats D, Schiby G, Gailani D, Levkovitz H, Avivi C, Tamarin I, Shaish A, Salomon O**. Factor XI Deficiency Protects Against Atherogenesis in Apolipoprotein E/Factor XI Double Knockout Mice. *Arterioscler Thromb Vasc Biol* 36: 475-481, 2016.

34. **Shupp JW, Prior SM, Jo DY, Moffatt LT, Mann KG, Butenas S**. Analysis of factor XIa, factor IXa and tissue factor activity in burn patients. *Burns* 44: 436-444, 2018.

35. **Steinberg SF**. The cardiovascular actions of protease-activated receptors. *Mol Pharmacol* 67: 2-11, 2005.

36. **Toullec D, Pianetti P, Coste H, Bellevergue P, Grand-Perret T, Ajakane M, Baudet V, Boissin P, Boursier E, Loriolle F, et al.** The bisindolylmaleimide GF 109203X is a potent and selective inhibitor of protein kinase C. *J Biol Chem* 266: 15771-15781, 1991.

37. **Tucker EI, Verbout NG, Leung PY, Hurst S, McCarty OJ, Gailani D, Gruber A.** Inhibition of factor XI activation attenuates inflammation and coagulopathy while improving the survival of mouse polymicrobial sepsis. *Blood* 119: 4762-4768, 2012.

38. **van Nieuw Amerongen GP, van Delft S, Vermeer MA, Collard JG, van Hinsbergh VW.** Activation of RhoA by thrombin in endothelial hyperpermeability: role of Rho kinase and protein tyrosine kinases. *Circ Res* 87: 335-340, 2000.

39. **Vellani V, Kinsey AM, Prandini M, Hechtfischer SC, Reeh P, Magherini PC, Giacomoni C, McNaughton PA.** Protease activated receptors 1 and 4 sensitize TRPV1 in nociceptive neurones. *Mol Pain* 6: 61, 2010.

40. **Vu TK, Hung DT, Wheaton VI, Coughlin SR.** Molecular cloning of a functional thrombin receptor reveals a novel proteolytic mechanism of receptor activation. *Cell* 64: 1057-1068, 1991.

41. **Wei C, Wang X, Chen M, Ouyang K, Song LS, Cheng H.** Calcium flickers steer cell migration. *Nature* 457: 901-905, 2009.

42. **Weitz JI, Fredenburgh JC.** 2017 Scientific Sessions Sol Sherry Distinguished Lecture in Thrombosis: Factor XI as a Target for New Anticoagulants. *Arterioscler Thromb Vasc Biol* 38: 304-310, 2018.

43. **Woodruff RS, Sullenger B, Becker RC.** The many faces of the contact pathway and their role in thrombosis. *J Thromb Thrombolysis* 32: 9-20, 2011.

44. **Yang L, Liu G, Zakharov SI, Morrow JP, Rybin VO, Steinberg SF, Marx SO.** Ser1928 is a common site for $Ca_V1.2$ phosphorylation by protein kinase C isoforms. *J Biol Chem* 280: 207-214, 2005.

45. **Zhao P, Metcalf M, Bunnett NW.** Biased signaling of protease-activated receptors. *Front Endocrinol* 5: 67, 2014.

Table 1. List of primers used in the RT-PCRs and real time PCRs

Primer		Sequences (5`-3`)	Tm (°C)*	Ta (°C)**	No***
S16	forward	ATATCCGGGTCCGTGTGA	63.9	60	35
	reverse	GAGATAGACTGCGGGATAGCA	63.1		
PAR$_1$	forward	TCTGACAATCGGAGAAAGGTG	64.1	60	35
	reverse	GGGTGTGTCTGTCTGTGCAA	64.1		
PAR$_2$	forward	GGGGATGCGAAGTCTCAG	63.5	60	35
	reverse	CAGACTTCTCCCTTTACTGTTGG	62.8		
PAR$_3$	forward	GATGAAAGTCCTTATCTTGGTTGG	63.5	60	35
	reverse	GCAGTTAAGGCTGAGTTGTCTG	62.8		
PAR$_4$	forward	ATGCTCGGGTTCAGCATC	63.9	60	35
	reverse	CTGTGGGACGCAGAGAGG	64.9		
Ca$_V$1.2	forward	ACTGCCAGCCCAGAAAAGAAA	66.9	65	40
	reverse	CAGGCGGAACCTGTTGTTTGG	70.6		
Ca$_V$1.3	forward	AAAGAAAGCCTAGAAAACAAA	56.4	55	40
	reverse	CACACGGATCGGGTTGGTCTT	70.3		
TRPC3	forward	GCATTCTCAATCAGCCAACA	63.8	60	40
	reverse	TTCACCTTCGTTCACCTCATC	64.0		
Orai1	forward	ATCGTCTTTGCCGTTCACTT	63.5	60	40
	reverse	AGAGAATGGTCCCCTCTGTG	63.1		
Orai2	forward	CGGAGAACTGGAGCCAAG	63.6	60	40
	reverse	ACTCATGGTGGGGACCAG	63.6		
Orai3	forward	CCACCAGTCACCACACCA	64.6	60	40
	reverse	CCAGCCCACCAAAACAAC	64.0		

* Melting Temperature (Tm) is calculated by a nearest neighbor method.

** Ta indicates annealing temperature.

*** No indicates cycle number in RT-PCR.

Table 2. The small interfering RNA (siRNA) sequences

Target	Sense strand (5`-3`)	Antisense strand (5`-3`)
Ca$_V$1.2	GGAAGAUUGCCCUGAAUGAdTdT	UCAUUCAGGGCAAUCUUCCdTdT
Orai1	GGGUGAAGUUCUUACCGCUdTdT	AGCGGUAAGAACUUCACCCdTdT
Orai2	GCCACAAGGGCAUGGAUUAdTdT	UAAUCCAUGCCCUUGUGGCdTdT
Orai3	GGAAAGGAGGCCCUAGUGAdTdT	UCACUAGGGCCUCCUUUCCdTdT

Figure legends

Figure 1. Intracellular Ca^{2+} signaling induced by FXIa, thapsigargin and PARs agonists in A7r5 cells.

Representative recordings and the summaries of the changes in cytosolic Ca^{2+} concentrations ($[Ca^{2+}]_i$) due to the Ca^{2+} release and Ca^{2+} influx observed with a Ca^{2+} add-back protocol in the absence (A) and presence of FXIa (B), thapsigargin (C), thrombin (D), TFLLR-NH_2 (E), trypsin (F) and SLIGRL-NH_2 (G) at the indicated concentrations in A7r5 cells. In this protocol, the cells were first exposed to Ca^{2+}-free media for 10 min (0 mM $[Ca^{2+}]_o$), and then stimulated with agonists or thapsigargin. After the transient $[Ca^{2+}]_i$ elevation (Ca^{2+} release component) returned to the pre-stimulation level, the extracellular Ca^{2+} was replenished to 2 mM (2 mM $[Ca^{2+}]_o$) in the presence of stimulation. After the sustained $[Ca^{2+}]_i$ elevation (Ca^{2+} influx component) was recorded for 10 min, the cells were exposed to 50 μM ionomycin in the presence of 1 mmol/mL extracellular Ca^{2+}. The Ca^{2+} responses were evaluated by the area under the trace and normalized by the peak elevation induced by 50 μM ionomycin. Thus, the values are expressed as arbitrary units (A.U.). The area under the trace of the Ca^{2+} release component was quantified from the time of stimulation to the time when the level of $[Ca^{2+}]_i$ returned to the pre-stimulation level. The area under the trace of the Ca^{2+} influx component was quantified by a 10-min trace, starting from the time of the replenishment of extracellular Ca^{2+}. The data are expressed as the mean ± SD. *$P < 0.05$, **$P < 0.01$ vs. control, according to an ANOVA followed by Dunnett's post-hoc test.

Figure 2. The involvement of PAR_1 in the Ca^{2+} responses induced by FXIa.

(A) A representative photograph of the RT-PCR (left, n = 3) and a summary of the real-time PCR (right, n = 3) of the mRNA expression of 4 subtypes of PARs in A7r5 cells are shown. The total RNA with no reverse transcription was used as template in RT-. In RT-PCR, the expression of S16 mRNA was evaluated as an internal control. In real-time PCR, the expression of PARs was quantified according to the standard curves obtained as described in the Materials and Methods section and then normalized by the level of S16 mRNA. (B) The concentration-dependent effects of atopaxar on the Ca^{2+} release and Ca^{2+} influx induced by 30 μM TFLLR-NH_2 in A7r5 cells. (C) The effects of 1 μM atopaxar on the Ca^{2+} release and Ca^{2+} influx induced by 30 μM SLIGRL-NH_2, 1 μM thapsigargin (TG) and 300 nM FXIa in A7r5 cells. (D) Representative recordings of the changes in $[Ca^{2+}]_i$ induced by 1 unit/mL thrombin, 30 μM TFLLR-NH_2 and 300 nM FXIa in the presence of 50 μM p-APMSF, a serine protease inhibitor, in A7r5 cells (n=3). In panels B and C, the Ca^{2+} responses are evaluated by the area under the trace as described in the legend of Figure 1. The data are expressed as the mean ± SD. *$P < 0.05$, **$P < 0.01$ vs. 30 μM TFLLR-NH_2 in the absence of atopaxar (B) or as indicated (B-C), according to an ANOVA followed by Bonferroni/Dunn post-hoc test. n.s., not significantly different.

Figure 3. The $[Ca^{2+}]_i$ elevations induced by thrombin, TFLLR-NH_2 and FXIa in wild-type and $PAR_1^{-/-}$ MEF.

Representative recordings of the changes in cytosolic Ca^{2+} concentrations ($[Ca^{2+}]_i$) induced by 30 μM TFLLR-NH_2 (n = 4), 1 unit/mL thrombin (n = 4), 300 nM FXIa (n = 4) and 1 μM thapsigagin (TG, n = 3) in wild-type ($PAR_1^{+/+}$) and $PAR_1^{-/-}$ MEF.

Figure 4. *In vitro* digestion of SUMOstar-PAR_1E-GST by thrombin and FXIa.

(A) The structure of the recombinant protein (SUMOstar-PAR_1E-GST), consisting of a N-terminal $(His)_6$-SUMOstar tag (108 amino acids, 12.3 kDa), the extracellular region of rat PAR_1 (PAR_1E, residues 22-109, 88 amino acids, 10.1 kDa) and a C-terminal glutathione S-transferase (GST) tag (225 amino acids, 26.3 kDa) is schematically shown with the expected two cleavage products by thrombin (SUMOstar-PAR_1E and PAR_1E-GST). (B)

Upper two photographs are the representative CBB-stained SDS-PAGE photographs showing the time course of digestion induced by 1 unit/mL thrombin and 300 nM FXIa (n = 3). Lower photograph is a photograph of CBB-stained SDS-PAGE gel containing the same samples used in the upper SDS-PAGE as indicated, in order to compare the size of cleavage products between thrombin and FXIa. IP1, input sample containing SUMOstar-PAR_1E-GST but no enzyme; IP2, input sample containing thrombin or FXIa but no SUMOstar-PAR_1E-GST. (C) The first four N-terminal amino acids of the PAR_1E-GST fragment obtained with 100-min digestion by thrombin and FXIa are shown.

Figure 5. The effects of Ca^{2+} channel blockers on the FXIa-induced Ca^{2+} influx.
(A) Representative recordings and summaries of the changes in $[Ca^{2+}]_i$ induced by 100 mM K^+ in the presence of 1 mM extracellular Ca^{2+} and with or without treatment with YM58483 (YM), Pyr3 and diltiazem at the indicated concentrations in A7r5 cells. The levels of $[Ca^{2+}]_i$ obtained at the peak and 8 min (plateau) after stimulation with 100 mM K^+ were normalized by the peak elevation obtained with 50 μM ionomycin. (B) Representative recordings and a summary of the changes in $[Ca^{2+}]_i$ induced by 1 μM thapsigargin (TG) with or without with Ca^{2+} channel blocker treatment in A7r5 cells. The Ca^{2+} channel blockers were applied at the time of replenishment of extracellular Ca^{2+}. The effects of Ca^{2+} channel blocker treatment were therefore evaluated by the levels of $[Ca^{2+}]_i$ obtained 8 min after the Ca^{2+} replenishment. (C) Summaries of the effects of Ca^{2+} channel blocker treatment on the Ca^{2+} influx component induced by 100 nM FXIa, 1 unit/mL thrombin and 30 μM TFLLR-NH_2 in A7r5 cells. The data are expressed as the mean ± SD. $*P < 0.05$, $**P < 0.01$ vs. the values obtained with stimulation in the absence of Ca^{2+} channel blockers, according to an ANOVA followed by Bonferroni/Dunn post-hoc test. n.s., not significantly different.

Figure 6. The mRNA expression of Ca^{2+} channels in A7r5 cells.

Representative RT-PCR images (n = 3) of Ca$_V$1.2, Ca$_V$1.3, TRPC3 and Orai1-3 are shown in A7r5 cells as well as brain, aorta, lung and kidney of normal rats. The estimated length of nucleotide of amplicon is shown in parenthesis.

Figure 7. The effects of knock-down of the expression of Ca^{2+} channels on the FXIa-induced Ca^{2+} influx.

(A) Summaries of the relative amounts of Ca$_V$1.2, Orai1, Orai2 and Orai3 mRNA in A7r5 cells, with or without (non) the transfection of 10 nM siRNA of negative control (NC), Ca$_V$1.2, Orai1, Orai2 and Orai3. The expression of Ca$_V$1.2, Orai1, Orai2, and Orai3 were quantified according to the standard curves obtained as described in the Materials and Methods section and then normalized by the level of S16 mRNA. (B) Summaries of the Ca^{2+} responses induced by 100 mM K^+, 1 μM thapsigargin, 1 unit/mL thrombin and 100 nM FXIa in A7r5 cells treated as shown in the panel A . The Ca^{2+} responses are evaluated by the level of $[Ca^{2+}]_i$ at peak and plateau (100 mM K^+) or the area under the trace (thapsigargin, thrombin and FXIa). The non-transfected cells did not receive any siRNA or Lipofectamine RNAiMAX. The data are expressed the mean ± SD. **P* < 0.05, ***P* < 0.01 vs. non-transfected cells or as indicated, #*P* < 0.05, ##*P* < 0.01 vs. NC, according to an ANOVA followed by Bonferroni/Dunn post-hoc test.

Figure 8. The effects of protein kinase inhibitors on the FXIa-induced Ca^{2+} influx.

(A, B) Summaries of the changes in the $[Ca^{2+}]_i$ induced by 100 mM K^+, 1 unit/mL thrombin, 30 μM TFLLR-NH_2 in the absence (vehicle) and presence of H89, LY294002 (LY), AZD0530 (AZD) and KN-93 (KN) (A) or presence of GF109203X (GF) and rottlerin (B) in A7r5 cells. (C) Summaries of the changes in the $[Ca^{2+}]_i$ induced by 100 nM FXIa in the absence (vehicle) and presence of H89, LY294002, AZD0530, KN-93, GF109203X and rottlerin in A7r5 cells. The Ca^{2+} responses were evaluated by the peak and plateau levels of $[Ca^{2+}]_i$ (100 mM K^+) or the area under the trace (thrombin and TFLLR-NH_2). Basal indicates the values obtained with no stimulation nor protein kinase inhibitor. The data are expressed as the mean ± SD. *$P < 0.05$, **$P < 0.01$ vs. Basal, #$P < 0.05$, ##$P < 0.01$ vs. Vehicle, according to an ANOVA followed by Bonferroni/Dunn post-hoc test.

Figure 9. The acceleration of cell migration induced by FXIa in A7r5 cells.
(A) Representative phase contrast microscopic images of A7r5 cell cultures obtain at 0 h and 10 h after applying a scratch wound. The dashed parallel lines indicate the edge of the wound. Scale bar: 250 μm. (B) Summary of the migration rate obtained within 10 h after the scratch wound under the indicated conditions. The data are expressed as the mean ± SD. *$P < 0.05$, **$P < 0.01$ vs. FXIa (-) without atopaxar or diltiazem; #$P < 0.05$, ##$P < 0.01$ vs. FXIa (+) without atopaxar or diltiazem, according to an ANOVA followed by Bonferroni/Dunn post-hoc test (B left) or Dunnett's post-hoc test (B right). n.s., not significantly different.

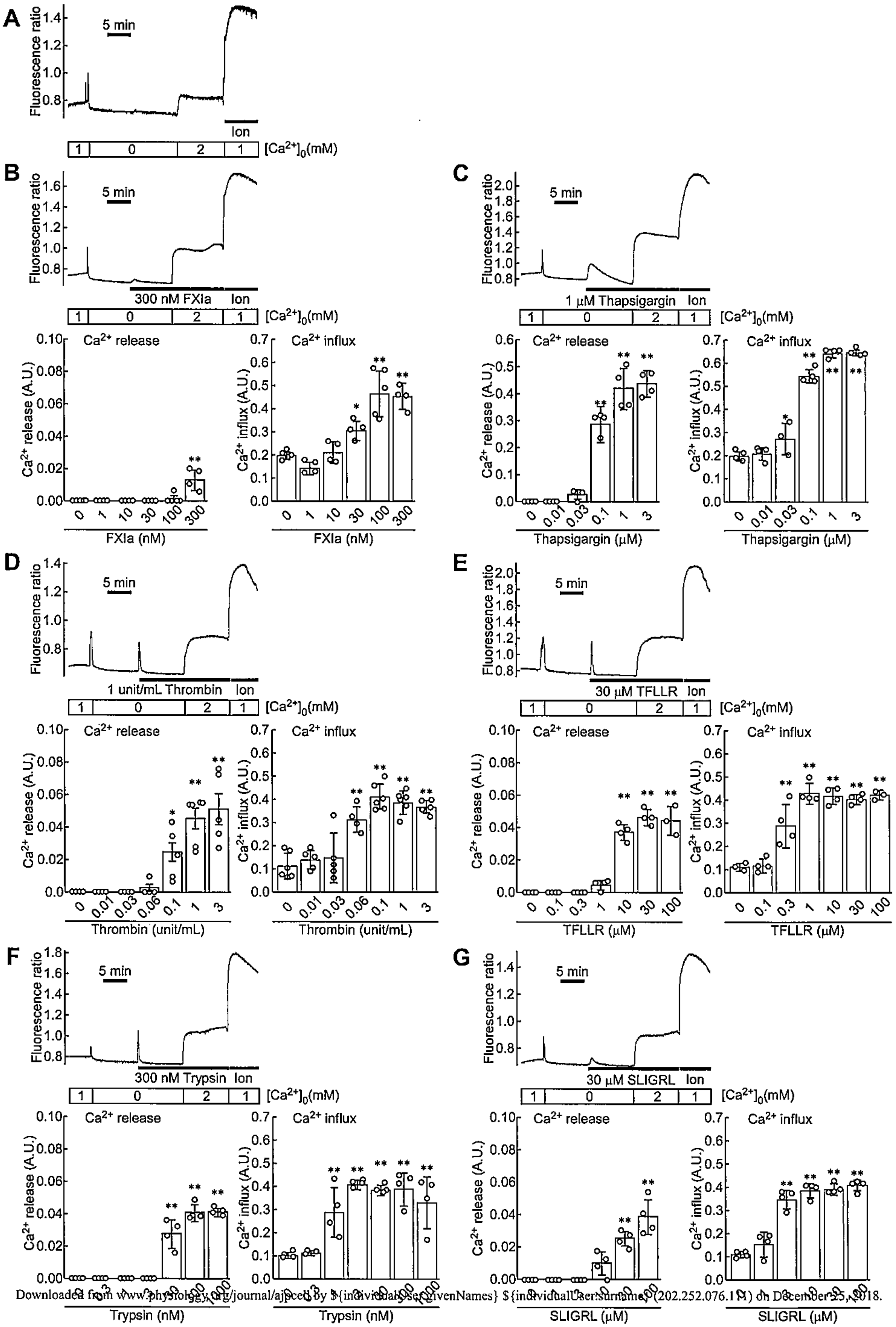

A
B
C
D
E
F
G
Fluorescence ratio
5 min
Ion
[Ca2+]0(mM)
300 nM FXIa
1 μM Thapsigargin
1 unit/mL Thrombin
30 μM TFLLR
300 nM Trypsin
30 μM SLIGRL
Ca2+ release
Ca2+ influx
Ca2+ release (A.U.)
Ca2+ influx (A.U.)
FXIa (nM)
Thapsigargin (μM)
Thrombin (unit/mL)
TFLLR (μM)
Trypsin (nM)
SLIGRL (μM)

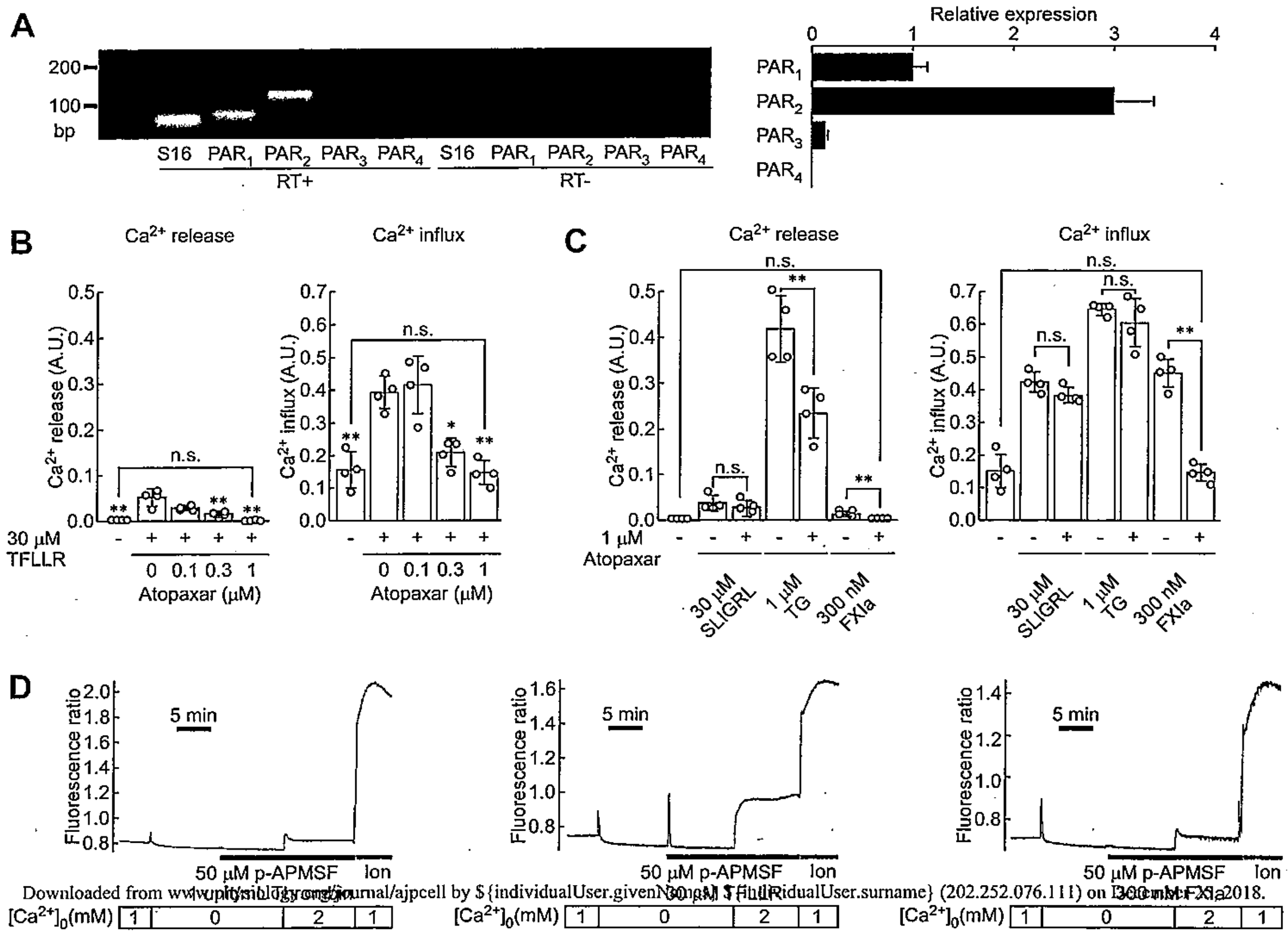
A
200
100
bp
S16 PAR1 PAR2 PAR3 PAR4 S16 PAR1 PAR2 PAR3 PAR4
RT+
RT-
Relative expression
PAR1
PAR2
PAR3
PAR4
B
Ca2+ release
Ca2+ influx
Ca2+ release (A.U.)
Ca2+ influx (A.U.)
30 µM TFLLR
Atopaxar (µM)
n.s.
C
Ca2+ release
Ca2+ influx
1 µM Atopaxar
30 µM SLIGRL
1 µM TG
300 nM FXIa
D
Fluorescence ratio
5 min
50 µM p-APMSF
Ion
[Ca2+]0(mM)

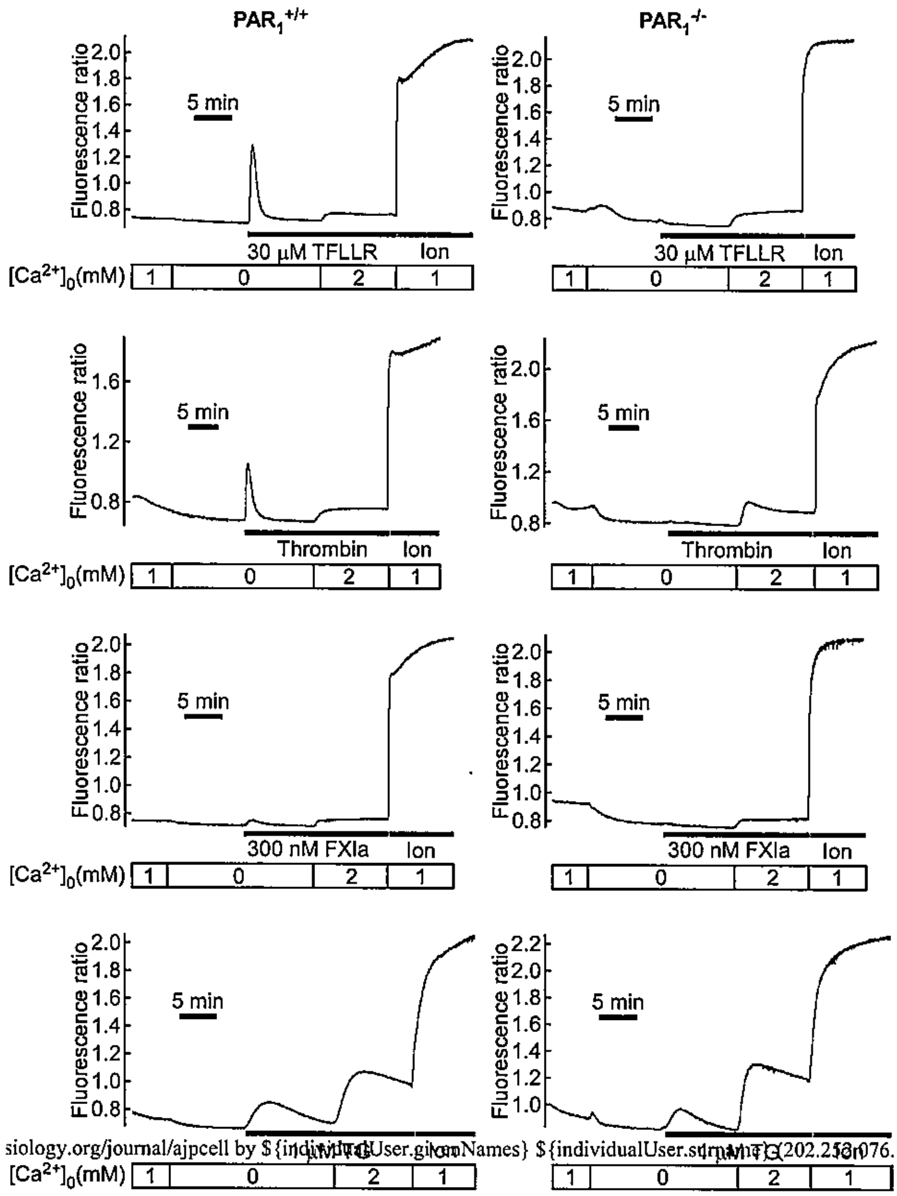
PAR$_1^{+/+}$
PAR$_1^{-/-}$
Fluorescence ratio
5 min
30 μM TFLLR
Ion
Thrombin
300 nM FXIa
[Ca^{2+}]$_0$(mM)
1
0
2
1
0.8
1.0
1.2
1.4
1.6
1.8
2.0
2.2

A

B

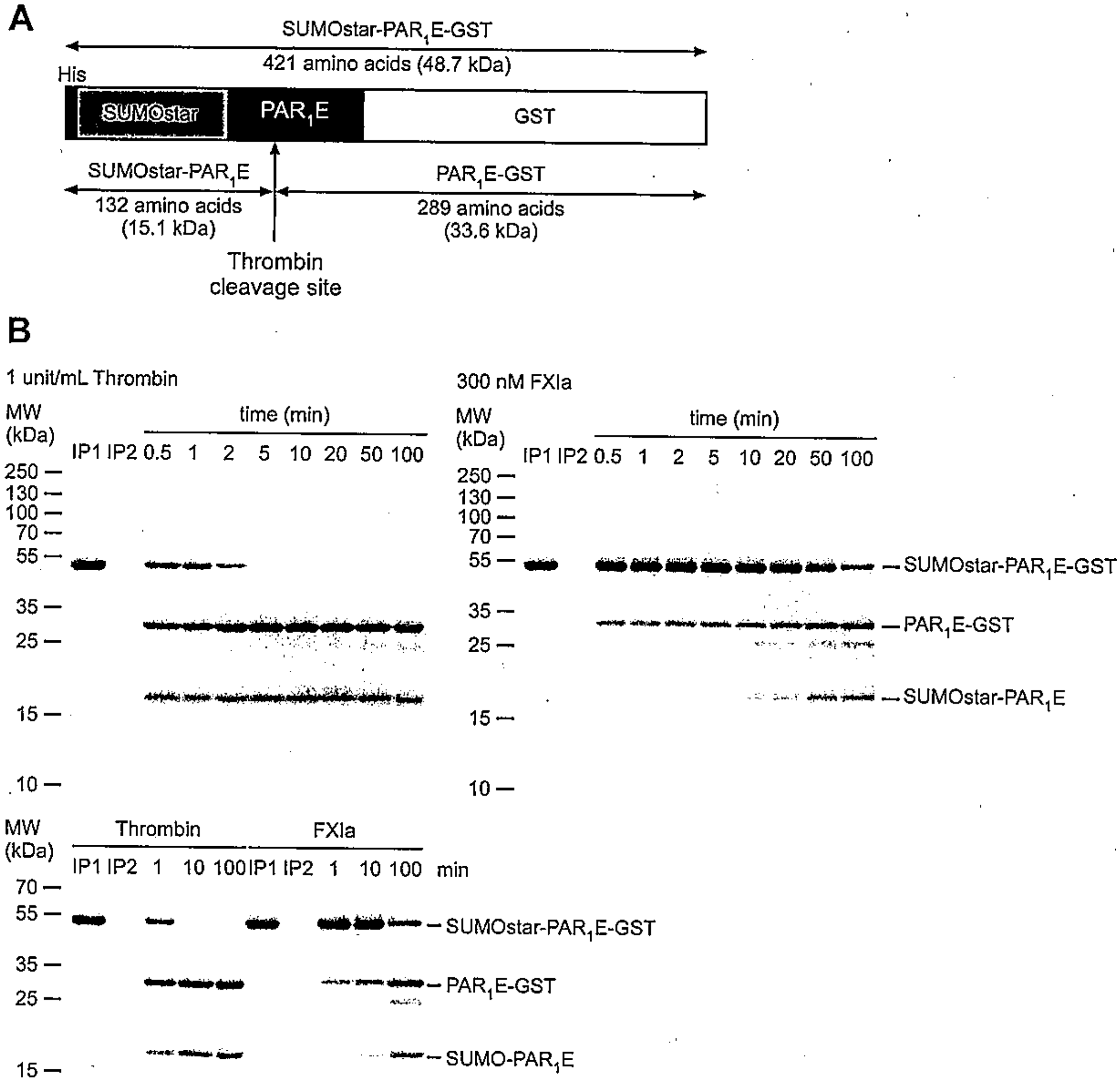

C

	1st	2nd	3rd	4th
Thrombin	S	F	F	L
FXIa	S	F	F	L

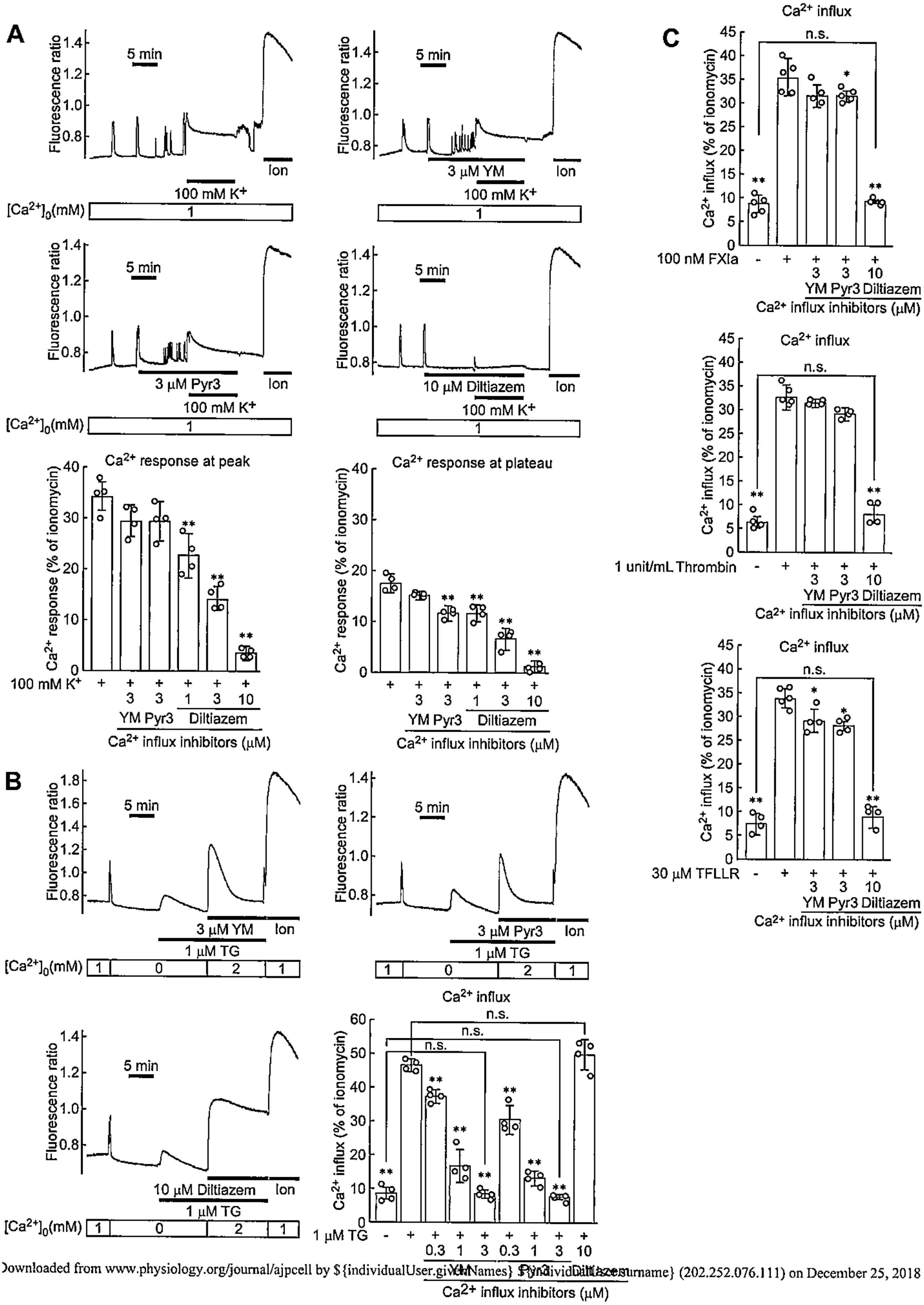

A
B
C
5 min
Fluorescence ratio
Ion
100 mM K+
3 μM YM
3 μM Pyr3
10 μM Diltiazem
[Ca2+]0(mM)
Ca2+ response at peak
Ca2+ response at plateau
Ca2+ response (% of ionomycin)
Ca2+ influx inhibitors (μM)
YM Pyr3 Diltiazem
1 μM TG
Ca2+ influx
Ca2+ influx (% of ionomycin)
n.s.
100 nM FXIa
1 unit/mL Thrombin
30 μM TFLLR

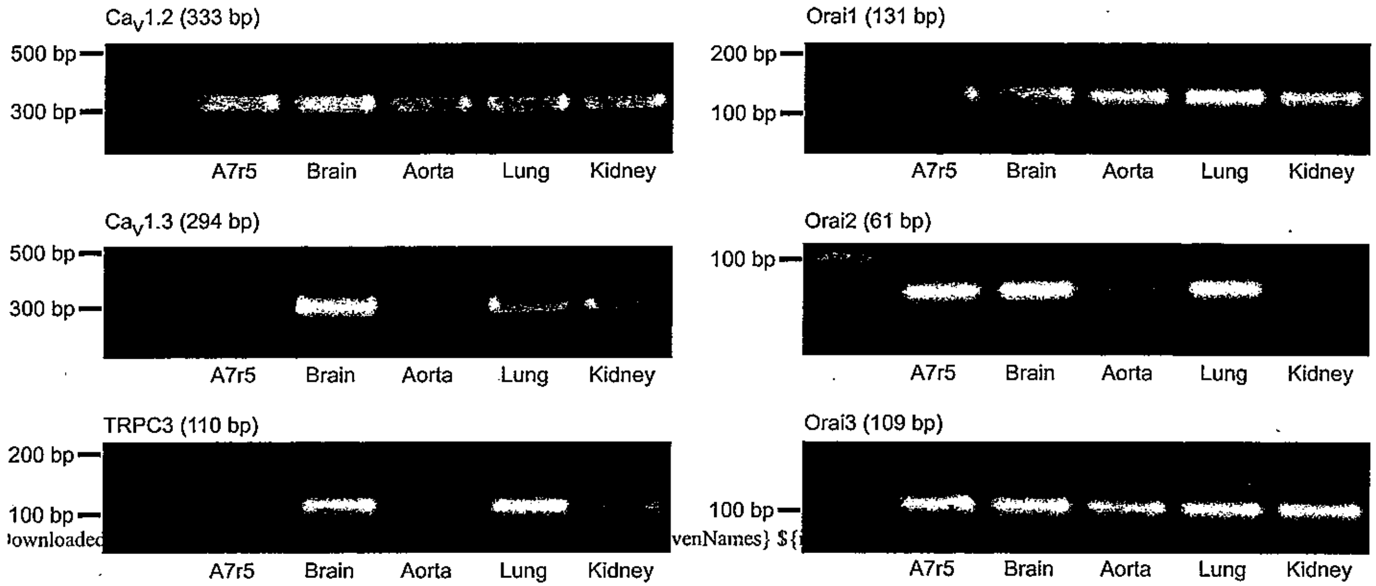

$Ca_V1.2$ (333 bp)
500 bp
300 bp
A7r5
Brain
Aorta
Lung
Kidney
Orai1 (131 bp)
200 bp
100 bp
A7r5
Brain
Aorta
Lung
Kidney
$Ca_V1.3$ (294 bp)
500 bp
300 bp
A7r5
Brain
Aorta
Lung
Kidney
Orai2 (61 bp)
100 bp
A7r5
Brain
Aorta
Lung
Kidney
TRPC3 (110 bp)
200 bp
100 bp
A7r5
Brain
Aorta
Lung
Kidney
Orai3 (109 bp)
100 bp
A7r5
Brain
Aorta
Lung
Kidney

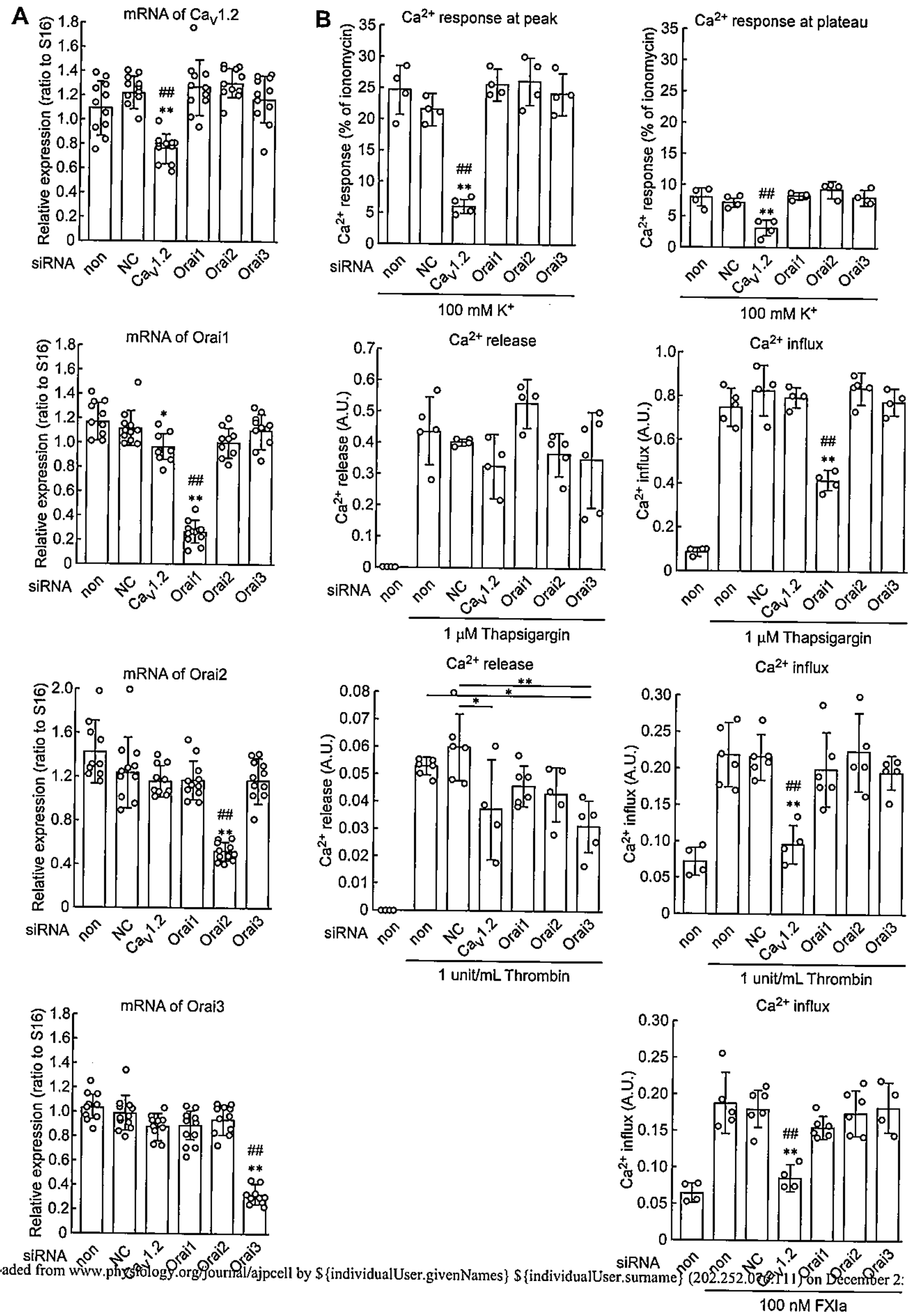

A
mRNA of $Ca_V1.2$
mRNA of Orai1
mRNA of Orai2
mRNA of Orai3
Relative expression (ratio to S16)
siRNA non NC $Ca_V1.2$ Orai1 Orai2 Orai3
B
Ca^{2+} response at peak
Ca^{2+} response at plateau
Ca^{2+} response (% of ionomycin)
100 mM K^+
Ca^{2+} release
Ca^{2+} release (A.U.)
Ca^{2+} influx
Ca^{2+} influx (A.U.)
1 μM Thapsigargin
1 unit/mL Thrombin
100 nM FXIa
siRNA non non NC $Ca_V1.2$ Orai1 Orai2 Orai3
##
**
*

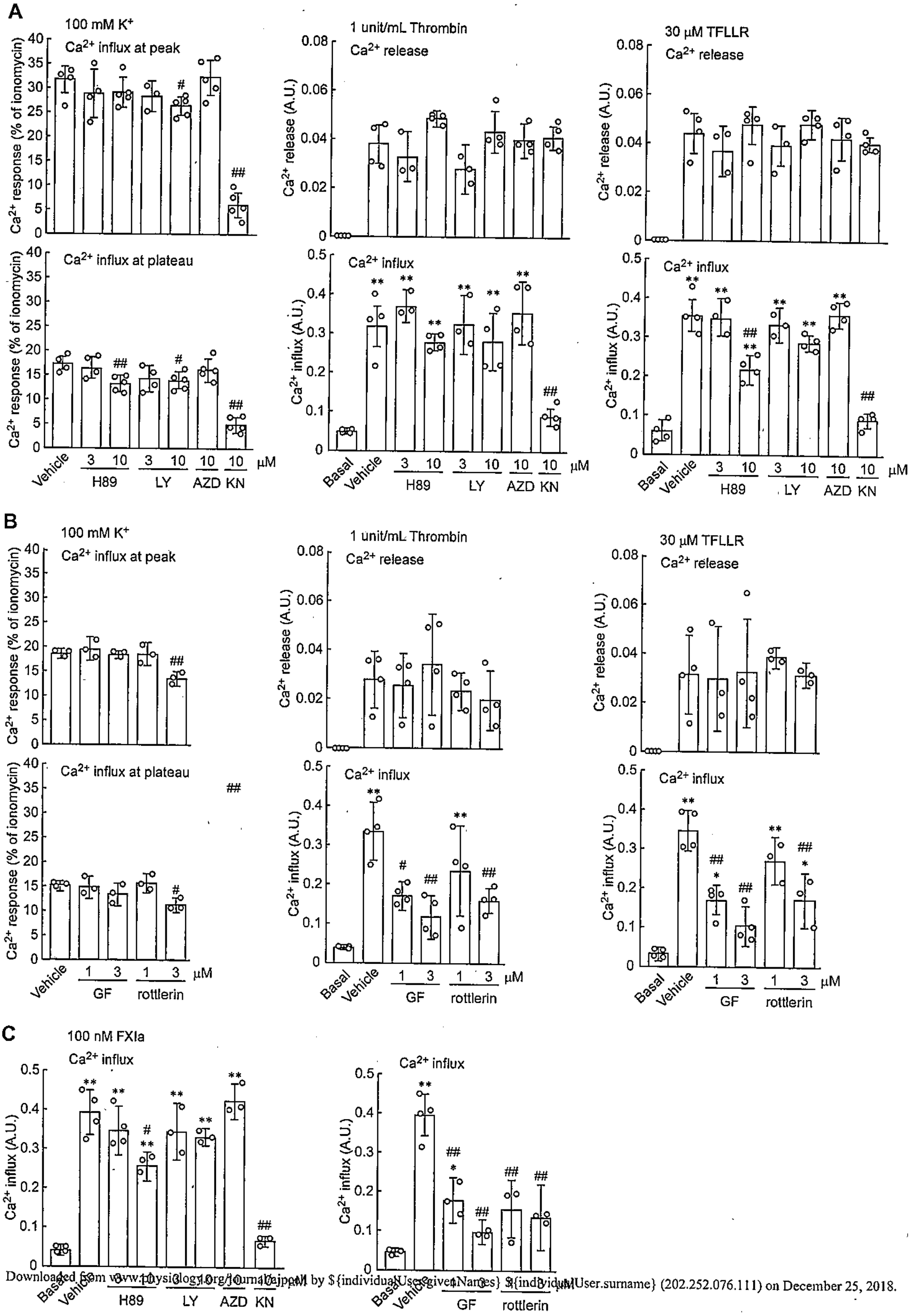
A
100 mM K+
Ca2+ influx at peak
Ca2+ response (% of ionomycin)
Ca2+ influx at plateau
Vehicle
3
10
H89
LY
AZD
KN
μM
#
##
1 unit/mL Thrombin
Ca2+ release
Ca2+ release (A.U.)
Ca2+ influx
Ca2+ influx (A.U.)
Basal
**
30 μM TFLLR
B
GF
rottlerin
1
*
C
100 nM FXIa

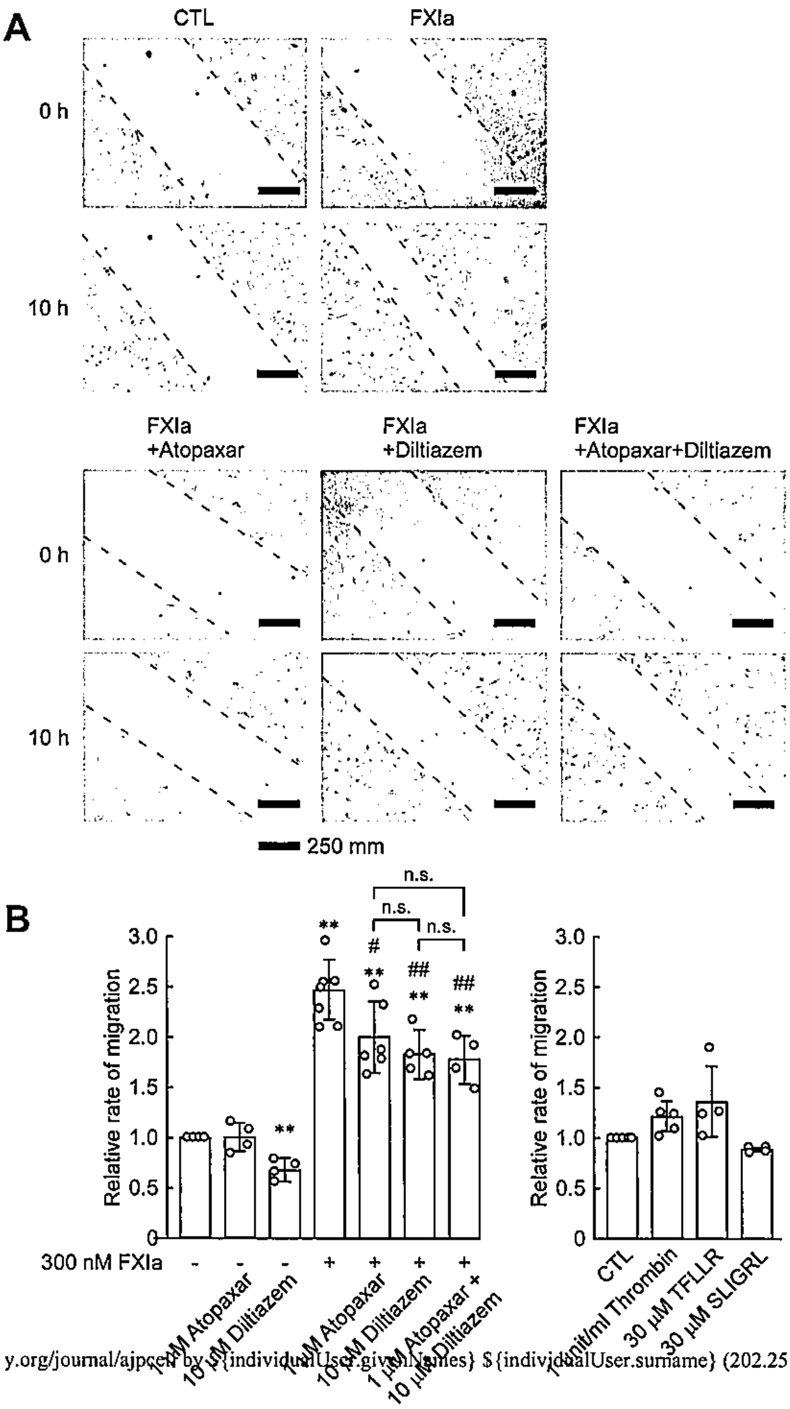
A
CTL
FXIa
0 h
10 h
FXIa
+Atopaxar
FXIa
+Diltiazem
FXIa
+Atopaxar+Diltiazem
0 h
10 h
250 mm
B
n.s.
n.s.
n.s.
Relative rate of migration
3.0
2.5
2.0
1.5
1.0
0.5
0
300 nM FXIa
1 μM Atopaxar
10 μM Diltiazem
1 μM Atopaxar
10 μM Diltiazem
1 μM Atopaxar +
10 μM Diltiazem
CTL
1 unit/ml Thrombin
30 μM TFLLR
30 μM SLIGRL